
Masters Theses

Student Theses and Dissertations

Fall 2012

Using LiDAR as a monitoring device to calculate volume of rockfall over time

Travis James Kassebaum

Follow this and additional works at: https://scholarsmine.mst.edu/masters_theses



Part of the [Geology Commons](#)

Department:

Recommended Citation

Kassebaum, Travis James, "Using LiDAR as a monitoring device to calculate volume of rockfall over time" (2012). *Masters Theses*. 5303.

https://scholarsmine.mst.edu/masters_theses/5303

This thesis is brought to you by Scholars' Mine, a service of the Missouri S&T Library and Learning Resources. This work is protected by U. S. Copyright Law. Unauthorized use including reproduction for redistribution requires the permission of the copyright holder. For more information, please contact scholarsmine@mst.edu.

USING LIDAR AS A MONITORING DEVICE TO CALCULATE
VOLUME OF ROCKFALL OVER TIME

by

TRAVIS JAMES KASSEBAUM

A THESIS

Presented to the Faculty of the Graduate School of the
MISSOURI UNIVERSITY OF SCIENCE AND TECHNOLOGY

In Partial Fulfillment of the Requirements for the Degree

MASTER OF SCIENCE IN GEOLOGICAL ENGINEERING

2012

Approved by

Norbert H. Maerz, Advisor
Jeffrey D. Cawlfeld
J. David Rogers

ABSTRACT

There are many natural hazards which threaten the stability of highway infrastructure and the safety of motoring public. Rockfall and unstable slopes are one of the major concerns. This thesis describes a method which safely and accurately evaluates rockfall on rock outcrops through the use of Light Detection and Ranging (LiDAR) data. LiDAR is an imaging technology which can be used to measure and evaluate possible rock outcrop hazards such as: rockfall, rock-avalanches, debris flows, and landslides. LiDAR produces a three dimensional point cloud of millions of points which gives spatial data on the scanned object, accurate to millimeters, in minutes. The point cloud can be exported to different formats which then can be analyzed using specialized software.

The software used for LiDAR data processing was developed here at Missouri University of Science and Technology using C++ with two open source libraries: OpenCV and OpenGL™. The program aligns two point clouds and calculates the volume found in between. The volume is the rockfall over time between the two scan dates used. The rockfall volume data is then correlated with rockfall triggering events, such as freeze and thaw cycles, precipitation levels, and seismic (blasting) data.

Very few rockfall volume correlations could be made with the rockfall triggering events at the outcrops tested, but further research should be done on the process with other types of rock outcrops. Some possible improvement areas are discussed in the last couple sections of this thesis. Also included are step-by-step instructions for reproducibility of the research.

ACKNOWLEDGMENTS

The completion of this thesis would not have been possible without the support and guidance from Dr. Norbert H. Maerz. Dr. Maerz inspired the author to continue education and research to pursue a master's degree. Dr. Maerz made all the work possible through funded research, which made a master's degree possible for the author. As an advisor, Dr. Maerz provided the needed support and guidance for the author's studies through the Geological Engineering program at Missouri S&T for both bachelor and master degrees. The author is forever grateful to Dr. Maerz for his everlasting support and friendship.

The author would also like to thank his committee members Dr. J. David Rogers and Dr. Jeffery D. Cawfield for their support and inspiration. Both Dr. Rogers and Dr. Cawfield helped inspire the author to continue with the master's program at Missouri S&T, and provided a never ending source of professional knowledge which will be beneficial for the rest of the author's life.

An extra special thanks to Ken Boyko for all his hard work on developing the computer processing used in the research, as well as his friendship and valuable knowledge which he provided.

The author is very grateful for his wonderful supporting family, especially his parents Dennis and Sandy, who made the author the person whom he is today. The author is also grateful for the love and support from his fiancé, Ally and her family, and all his close friends, especially Josh, Kerry, and James, who have motivated and encouraged the author when it has been needed.

This thesis could not have been done without all the help and support provided to the author from everybody.

TABLE OF CONTENTS

	Page
ABSTRACT	iii
ACKNOWLEDGMENTS	iv
LIST OF ILLUSTRATIONS	viii
LIST OF TABLES	x
SECTION	
1. INTRODUCTION	1
1.1. INTRODUCTION	1
1.2. OBJECTIVES	2
1.3. THESIS ORGANIZATION	2
2. BACKGROUND INFORMATION	3
2.1. INTRODUCTION	3
2.2. SLOPE STABILITY	3
2.2.1. Rockfall	3
2.2.1.1 Wedge failure	4
2.2.1.2 Plane failure	5
2.2.1.3 Toppling failure	6
2.2.1.4 Raveling failure	7
2.2.2. Dealing with Rockfall	7
2.3. LIDAR BACKGROUND	8
2.3.1. Three-Dimensional Laser Scanners	8
2.3.1.1 Time-of-flight	8
2.3.1.2 Phase-shift	9
2.3.1.3 Comparison	9
2.3.2. Point Cloud Data	10
2.3.2.1 Point data	10
2.3.2.2 Point data plus intensity	11
2.3.2.3 Point data plus color value	11
2.4. USING LIDAR FOR SLOPE STABILITY ANALYSIS	12

3. METHODOLOGY	15
3.1. INTRODUCTION	15
3.2. SITE SELECTION	16
3.3. DATA ACQUISITION	18
3.3.1. Equipment Needed	18
3.3.2. Equipment Setup	19
3.3.3. Setting Parameters	21
3.3.4. Scanning	23
3.3.5. Exporting Data	24
3.4. DATA PROCESSING	24
3.4.1. Data Process	24
3.4.1.1 Pre-load	24
3.4.1.2 Load	24
3.4.1.3 Fill gaps.....	25
3.4.1.4 Registration	26
3.4.1.5 Vegetation detection and removal	28
3.4.1.6 Difference surface creation	29
3.4.1.7 Rock segmentation.....	30
3.4.1.8 Volume determination	32
3.4.2. Production and Development Environment	32
3.4.2.1 Directory structure	32
3.4.2.2 Parameter tuning	32
3.4.2.3. Batch scripts.....	33
3.4.2.4. Batch log files	33
3.4.2.5. Back-ups.	33
3.5. VOLUME ACCURACY	33
3.5.1. Water Immersion Test	33
3.5.2. Clay Rockfall Simulation	35
3.6. GEOLOGY, ROCK MASS RATING, AND Q RATING OF SITES.....	38
3.6.1. Introduction	38
3.6.2. Rock Mass Rating	39

3.6.3. Rock Tunneling Quality Index	40
4. DATA CORRELATION, RESULTS, AND CONCLUSION	43
4.1. INTRODUCTION	43
4.2. DATA	43
4.2.1. Rockfall Volume	43
4.2.2. Freeze and Thaw Cycles.....	46
4.2.3. Precipitation Levels.....	47
4.2.4. Seismic Data.....	48
4.3. FINAL RESULTS AND POSSIBLE DATA IMPROVEMENTS.....	48
4.3.1. Data Correlation	48
4.3.2. Possible Method Improvements	53
4.3.2.1 Improved scanner setup	53
4.3.2.2 Parameter sensitivity analysis	53
4.3.2.3 Improved registration process.....	54
4.3.2.4 Other ideas to be considered	54
4.4. CONCLUSION.....	55
APPENDICES	
A. STEP-BY-STEP INSTRUCTIONS FOR DATA COLLECTION.....	56
B. DATA PROCESSING SOURCE CODE.....	60
BIBLIOGRAPHY	66
VITA.....	68

LIST OF ILLUSTRATIONS

	Page
Figure 2.1. Example of Different Failures	3
Figure 2.2. Diagram of a Wedge Failure	5
Figure 2.3. Diagram of a Plane Failure.....	6
Figure 2.4. Diagram of a Toppling Failure.....	7
Figure 2.5. Image of LiDAR Scanners Used in Project.....	8
Figure 2.6. Point Cloud in XYZ Format	11
Figure 2.7. Point Cloud in XYZI Format.....	12
Figure 2.8. Point Cloud in XYZRGB Format.....	12
Figure 3.1. Map of Study Sites Relative to Rolla, Missouri.....	15
Figure 3.2. Map of Study Sites	16
Figure 3.3. Site 1 Setup.....	17
Figure 3.4. Site 2 Setup.....	18
Figure 3.5. Site 1 Marker	19
Figure 3.6. Site 2 Marker	20
Figure 3.7. Tribrach	21
Figure 3.8. Field of View Extent of Site 1	22
Figure 3.9. Field of View Extent of Site 2.....	23
Figure 3.10. Outcrop Data Before and After the Fill Gap Function.....	26
Figure 3.11. Split Screen Registration Process.....	27
Figure 3.12. Vegetation Removal Filter	29
Figure 3.13. Example of Successful Vegetation Removal	30
Figure 3.14. Raw Difference Surface Image	31
Figure 3.15. Rock Which is Used for Volume Test.....	34
Figure 3.16. Water Immersion Volume Test	34
Figure 3.17. Air Gap Measurement	35
Figure 3.18. Clay Rockfall Simulation Test Setup	36
Figure 3.19. Rock Outcrop for Clay Test	38
Figure 3.20. Site 1 Rock Outcrop Separated into Three Areas.....	39

Figure 3.21. Site 2 Rock Outcrop	41
Figure 4.1. Rockfall Volume Calculated Using LiDAR.....	44
Figure 4.2. Location of Rockfall Volume.....	45
Figure 4.3. Freeze and Thaw Cycles Recorded During Each Sampling Interval	46
Figure 4.4. Recorded Precipitation Levels During Each Sampling Interval.....	47
Figure 4.5. Seismic (Blasting) Data.....	49
Figure 4.6. Site 1 Data Correlations.....	51
Figure 4.7. Site 2 Data Correlations.....	52

LIST OF TABLES

	Page
Table 2.1. Comparison of Time-of-Flight and Phase-Shift Scanners.....	10
Table 2.2. Afternoon Creek, Washington LiDAR Data.....	14
Table 3.1. Distribution of Data Points	25
Table 3.2. LiDAR Vs Water-Immersion Volume Comparison	36
Table 3.3. Clay Rock Simulation Results	37
Table 4.1. Julian Dates.....	43

1. INTRODUCTION

1.1. INTRODUCTION

Quantifying volume of rockfall has often been done by estimating how much rock is removed from the ditch periodically, as needed, typically with no set schedule for ditch cleaning. The method described in this thesis presents the idea of using LiDAR as an engineering tool to quantify the amount of rockfall over time by the use of monitoring. The rockfall volume is found by comparing LiDAR point clouds to one another and finding the difference between two subsequent point clouds that have been registered to one another. Erroneous data such as cars passing by, dust particles, or vegetation that come between the scanner and the rock slope during scanning is removed by using automated methods.

Volume of material lost data gathered by LiDAR can be compared to external events to find correlations with rockfall occurrences. The data contained in this thesis is compared to freeze thaw cycles, precipitation levels, and seismic (blasting) data for rockfall volume correlation.

One of the most advantageous reasons for using LiDAR as a slope stability tool is the fact that multiple objectives can be found from one simple set of scans. Using LiDAR requires a minimum of one scan in the field lasting anywhere from 5 to 30 minutes depending on the size and resolution of the area. However, from the few minutes spent in the field gathering data, enormous amounts of information can be found from the data back in the office. In addition to the rockfall volume estimation which this thesis will cover, other aspects are being researched for slope stability and the use of LiDAR. Areas such as discontinuity orientation and discontinuity roughness can also be applied using the same set of LiDAR data. Since the use of LiDAR for monitoring requires multiple scans taken over a period of time, it is even possible to determine joint orientation shifts and rotations, or distance of creep movement.

1.2. OBJECTIVES

The objective of this research project is to show the capabilities of using LiDAR as a monitoring tool for rock slope stability by quantifying the volume and sequence of rockfall over a period of time.

1.3. THESIS ORGANIZATION

This thesis report comprises of four Sections:

Section 1 provides an introduction, objectives, and an overview of the thesis organization.

Section 2 presents background information, including the significance of slope stability and different types of slope failure mechanisms, LiDAR background and type of data acquired.

Section 3 presents the methodology of the work completed, summarizing the data acquisition and data processing methods. This section also includes specific parameters used at each site location. Additionally two tests were done for testing the data processing and have been included at the end of this section.

Section 4 presents the data after processing. This section compares the volume changes found to other external parameters to help find a correlation in the cause of rockfall. Suggestions for improvements and future research as well as final conclusion is also included in this section.

2. BACKGROUND INFORMATION

2.1. INTRODUCTION

This research attempts to demonstrate the capabilities of using LiDAR as a slope stability evaluation tool. Human bias is a large problem when using other techniques of quantifying rockfall and determining overall slope stability, which by using LiDAR as an everyday tool can be removed. Background research has been completed to give a clearer understanding of the potential problem, slope stability, and of LiDAR and how it could be used in evaluating rock slopes.

2.2. SLOPE STABILITY

Ground movement and slope instability are issues which may affect the safety of both motorists and the highway infrastructure. Rockfall is the most common problem, as it happens the most frequently. This section will discuss the different types of rockfall and possible ways to deal with the problem.

2.2.1. Rockfall. Rockfall describes a process by which rock falls freely from an exposed outcrop due to gravity. The four primary types of rockfall are: wedge, planar sliding, toppling, or raveling. Figure 2.1 shows these four types of rockfall.



Figure 2.1. Example of Different Failures. Wedge (far left), Planar Sliding (middle left), Toppling (middle right), and Raveling (far right) (Maerz, 2012).

According to Franklin and Senior (1997b) only 33% of 415 failures studied in Northern Ontario were of the first three types. Throughout these sites studied, 65% of the failures were considered to be of raveling type failure. Specifically 25% raveling, 15% overhand/undercutting failure, 14% ice jacking, and 11% rolling blocks were the cause of rockfall. The rock may roll, bounce, or slide from the outcrop, possibly landing on the road and causing major issues. A rockfall is different than a rock avalanche, in that a rock avalanche is greater than 10^5 cubic meters of rock material which moves with flow-like characteristics (Holm and Jakob, 2009). Rockfall typically has a relatively low magnitude when compared with other landslide processes, but due to its frequency it poses a significant threat to motoring public and infrastructure. Hungr and Evans (1989) noted that there has been a total of 13 rockfall related deaths in the past 87 years in Canada.

Most often rockfalls are initiated by some climatic or biological event. These type of events may include pore pressure increases, erosion of surrounding material, freeze-thaw ice wedging, chemical degradation or weathering, or wedging from root growth. Once the movement of a rock has been started, the fall trajectory is controlled primarily by the geometry of the slope. The most dangerous type of rockfalls are those which the rock "ski-jumps"; having high horizontal velocity and bouncing and rolling a long way away from the toe of the slope (Hoek, 2000). While clean, freshly cut and smooth surface, unweathered rock slopes typically have lower quantities of rockfall, they are sometimes more dangerous because the fresh rock surfaces don't allow for any retardation of the falling rock which a weathered surface may provide. The retarding capacity of the surface material is known as the coefficient of restitution, and is dependent on the nature of the material that forms the impact surface. For this reason gravel benches which have a low coefficient of restitution are often used in order to prevent further bouncing of falling rocks.

2.2.1.1 Wedge failure. Wedge failures can occur over a wide range of geometric conditions. They are formed by two continuous planar discontinuities and the line of intersection of the two daylight planes above the toe of the rock face. The geometric conditions which are typical for wedge failures described by Wyllie and Mah (2004) are as follows:

- Two planes will intersect in a line. On a stereonet the line of intersection is represented by a vector where two great circles intersect, and the orientation of the line is found by its trend and plunge.
- The plunge of the line of intersection must be flatter than the dip of the face, and greater than the average friction angle of the two slide planes.
- The line of intersection must dip in the direction out of the face.

Figure 2.2 shows a diagram of a wedge failure.

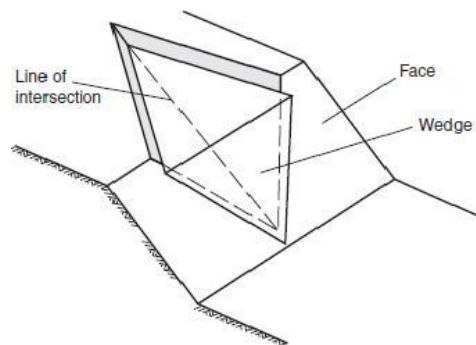


Figure 2.2. Diagram of a Wedge Failure (Wyllie and Mah, 2004).

2.2.1.2 Plane failure. Plane failures are quite rare in rock slopes because they require specific geometry conditions of two dimensions. Wyllie and Mah (2004) summarize the description of the required plane failure condition:

- The plane on which the sliding occurs must strike parallel or nearly parallel to the slope face.
- The sliding plane must daylight in the slope face, which means that the dip of the plane must be less than the dip of the slope face.
- The dip of the sliding plane must be greater than the angle of friction of this plane.
- The upper end of the sliding surface either intersects the upper slope, or terminates in a tension crack.

- Release surfaces that provide negligible resistance to sliding must be present in the rock mass to define the lateral boundaries of the slide. Alternatively, failure can occur on a sliding plane passing through the convex “nose” of a slope.

Figure 2.3 shows a diagram of a plane failure.

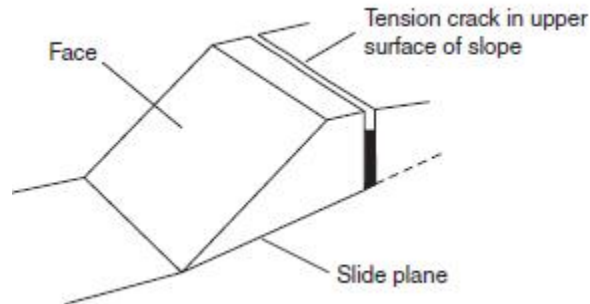


Figure 2.3. Diagram of a Plane Failure (Wyllie and Mah, 2004).

2.2.1.3 Toppling failure. Toppling failure is quite different when compared to either wedge or sliding failures. Toppling involves the rotation of columns or blocks of rock about a fixed base. Goodman and Bray (1976) specify two main types of toppling, block toppling and flexural toppling. Block toppling occurs in strong rock when individual columns are formed by a set of discontinuities dipping steeply into the face, and a second set of widely spaced orthogonal joints defines the column height, such as bedded sandstone or columnar basalt. The shorter columns forming the toe of the slope are pushed by the loads from the overturning columns behind, and the sliding of the toe causes block toppling to occur. Flexural toppling is similar to block toppling, except the steeply dipping discontinuities often break in flexure as they bend forward, toppling over, such as in thinly bedded shale and slate. Sliding, excavation or erosion of the toe of the slope will often trigger the toppling process, and will domino effect back into the rock mass (Wyllie and Mah, 2004). Figure 2.4 shows a diagram of a toppling failure.

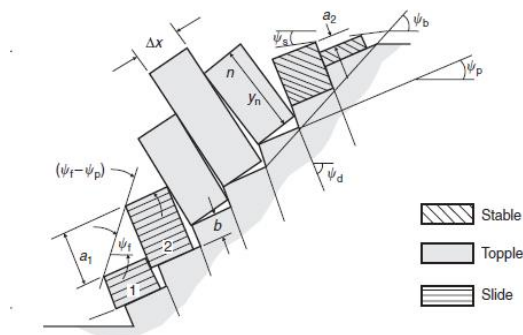


Figure 2.4. Diagram of a Toppling Failure (Wyllie and Mah, 2004).

2.2.1.4 Raveling failure. Raveling failure is very different from the other three failures mentioned before. Raveling isn't necessarily dependent on the geometry of the site, or the orientation of the planes, it is typically caused by weathering of the rock and is time dependent. As previously mentioned it is the most common type of rockfall, and often only small blocks are released. Raveling can also cause large, catastrophic failures, depending on the size of blocks which are released. Some of the worse failures are when undercutting (type of raveling) causes entire slope failure (Maerz, 2012).

2.2.2. Dealing with Rockfall. It is impossible to detect all rockfall hazards before they occur. Some hazards, such as large boulders at the edge of a slope, are obvious, but others which appear to be a stable rock face until a small block is released causing a cascading slope failure. The release of some of the smaller blocks may cause a chain reaction creating more rockfall or in some instances, large scale slope failure (Hoek, 2000). To aid in determining the hazard and potential impact of possible rockfall, many places in the US and Canada have created rockfall hazard assessments, one of the most widely accepted being the Rockfall Hazard Rating System (RHRS) which was developed by the Oregon State Highway Division (Pierson et al. 1990). By using such a system it can better be determined which locations may need the most attention the soonest. Using a rating system can also help determine what kind of methods may be needed to solve the problems in each specific location. The use of LiDAR as a slope stability tool is a new option, which could provide significant data on orientation of joints as well as a monitoring tool for calculating volume of rockfall over a period of time.

2.3. LIDAR BACKGROUND

LiDAR, which stands for light detection and ranging, is a laser scanner which collects data and produces an accurate three-dimensional point cloud. As technology advances improved LiDAR systems and software are being developed which are more accurate and easier to use. This section will discuss the different types of LiDAR being used and researched today, as well as general LiDAR information.

2.3.1. Three-Dimensional Laser Scanners. LiDAR collects data by emitting laser light and detecting the reflection of the laser to determine the distance from the scanner to the scanned object. It works much like that of a laser rangefinder, except laser scanners use rotating mirrors to gather millions of measurements in a short amount of time. There are two primary types of laser scanners, time-of-flight and phase-shift, both of which collect similar data. Figure 2.5 shows a picture of the ScanStation2 (time-of-flight) and the HDS6000 (phase-shift) LiDAR scanners.



Figure 2.5. Image of LiDAR Scanners Used in Project. ScanStation2 (Left) and HDS6000 (Right) (Leica Geosystems).

2.3.1.1 Time-of-flight. Time-of-flight laser scanners emit a pulse of laser light which is then reflected off the object. A sensor measures the time of flight of the pulse which is used to accurately measure the distance from the LiDAR to the object. The distance is found by the following equation:

$$Distance = \frac{(Speed\ of\ Light * Time\ of\ Flight)}{2} \quad (1)$$

2.3.1.2 Phase-shift. Phase-shift laser scanners use a laser beam with sinusoidally modulated optical power which is reflected off an object. A sensor then detects and compares the reflected light with the emitted light to determine the phase shift. After that the time-of-flight is calculated using the following equation:

$$Time\ of\ Flight = \frac{Phase\ Shift}{(2\pi * Modulation\ Frequency)} \quad (2)$$

After the time-of-flight is calculated, equation one is then used to calculate the distance using the time-of-flight.

2.3.1.3 Comparison. While both time-of-flight and phase-shift scanners collect identical data, there are differences between the two. Time-of-flight scanners can typically scan at greater distances with more accuracy when compared to the phase-shift scanners. This makes time-of-flight scanners more desirable for use along large highway slopes and cliffs whereas the phase shift scanners might be more useful in smaller areas such as underground tunnels or inside buildings. The phase shift scanners are able to acquire data more quickly just at a lesser range. Phase-shift scanners are typically much smaller and lighter when compared to that of the time-of-flight scanners. Even the batteries of most phase-shift scanners are located within the laser scanner, whereas the batteries of a time-of-flight scanner are typically external and much larger. This makes using phase-shift scanners easier and faster, although the distance is limited. As the technology increases, so will the capabilities and user-friendly aspects of the two different types of scanners (Ground-Based LiDAR, 2008). Table 2.1 was prepared by Point of Beginnings website comparing a time-of-flight and phase-shift LiDAR scanners.

Table 2.1. Comparison of Time-of-Flight and Phase-Shift Scanners (POB, 2008).

Parameter	Optec ILRIS 3D (time of flight)	Leica HDS6000 (phase shift)
Wavelength	1550 nm	650, 690 nm
Minimum range	3 m	0.1 m
Maximum range	1500 m at 80% reflectivity	79 m at 90% reflectivity
Average data acquisition rate	2500 points per second	125,000 points per second
Beam diameter	29 mm @ 100 m	8 mm @ 25 m
Distance accuracy	7 mm @ 100 m	4 mm @ 25 m
Position accuracy	8 mm @ 100 m	6 mm @ 25 m
Angular accuracy	0.00115 degrees	0.0071 degrees
Scanner weight	13 kg not including batteries	14 kg including batteries
Distance and position accuracies are ± 1 sigma (68% confidence level)		

2.3.2. Point Cloud Data. Of the LiDAR systems available today, there are three primary point cloud data formats which the internal data is exported to for analysis. The data which is received can be viewed in any of the formats, depending the the capabilities of the particular LiDAR scanner being used. The three formats are:

- Point data (XYZ)
- Point data plus intensity (XYZI)
- Point data plus color value (XYZRGB)

In addition to the three formats listed, the data is sometimes exported as point data with intensity and color values assigned (XYZIRGB). This type of data requires the most computational power, as well as is the most informative. The point clouds used for this thesis are of this format, simply for more available information if needed and the ability to best display the data.

2.3.2.1 Point data. The point data which is gathered is simply the point in space. Each point which is scanned will give an XYZ coordinate relative to the LiDAR scanner. This particular data has no variation in the color of the points. It is the least demanding type of format for computational requirements and data storage, as the only data is the point in space. This type of format is the most challenging for the human eye to distinguish. Figure 2.6 is an example of a point cloud in XYZ format.

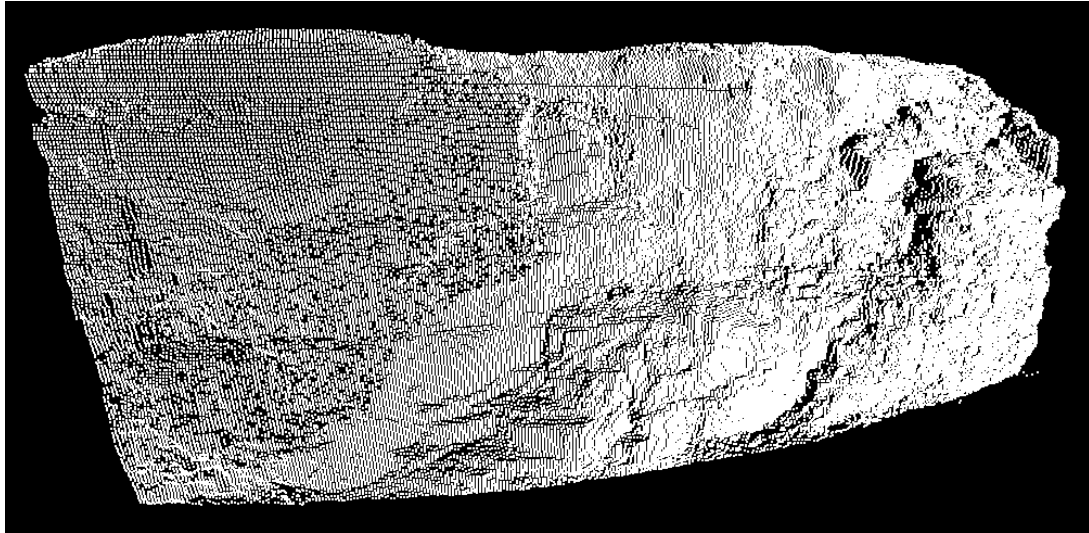


Figure 2.6. Point Cloud in XYZ Format (Site 1).

2.3.2.2 Point data plus intensity. Data of XYZI format is very similar to the XYZ data except it includes an intensity value which is directly related to the reflectivity of a scanned object. The additional information adds to the complexity of the data, requiring slightly more computational requirement and data storage. The intensity value does increase the visibility of the point cloud depth and perspective. Figure 2.7 is an example of a point cloud in XYZI format.

2.3.2.3. Point data plus color value. Data of XYZRGB format has additional color values obtained from high resolution cameras. Depending on the LiDAR scanner, sometimes the scanner has a built in camera where all the data can be gathered using just the LiDAR, while other scanners do not have a built in camera but have the capability to add photo colors to the point cloud using a special external camera. The photo enhanced data does increase the data size even more than the point data with intensity values. This type of data is the easiest to determine the depth and perception of the point cloud.

Figure 2.8 is an example of a point cloud in XYZRGB format.

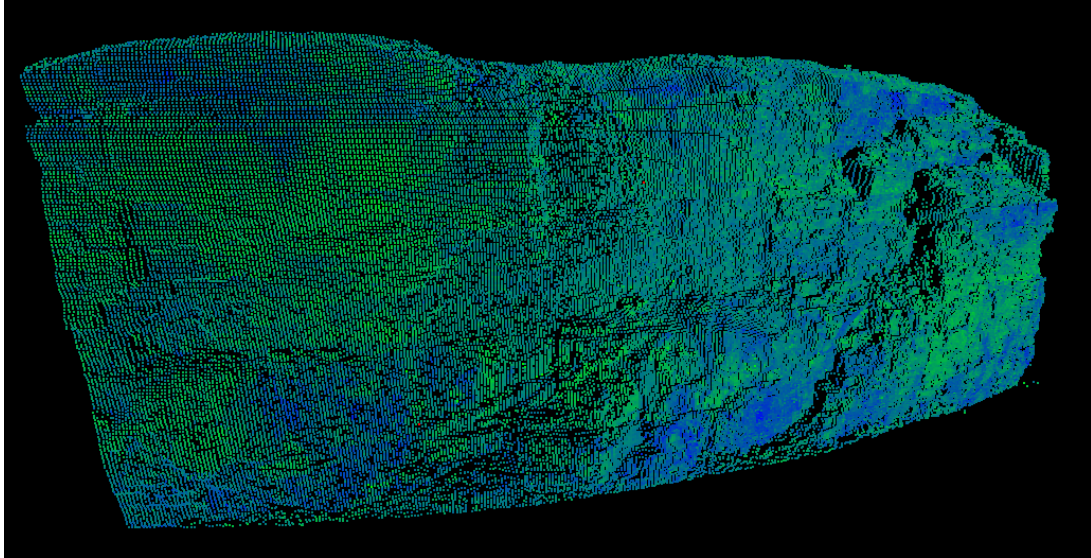


Figure 2.7. Point Cloud in XYZI Format (Site 1).

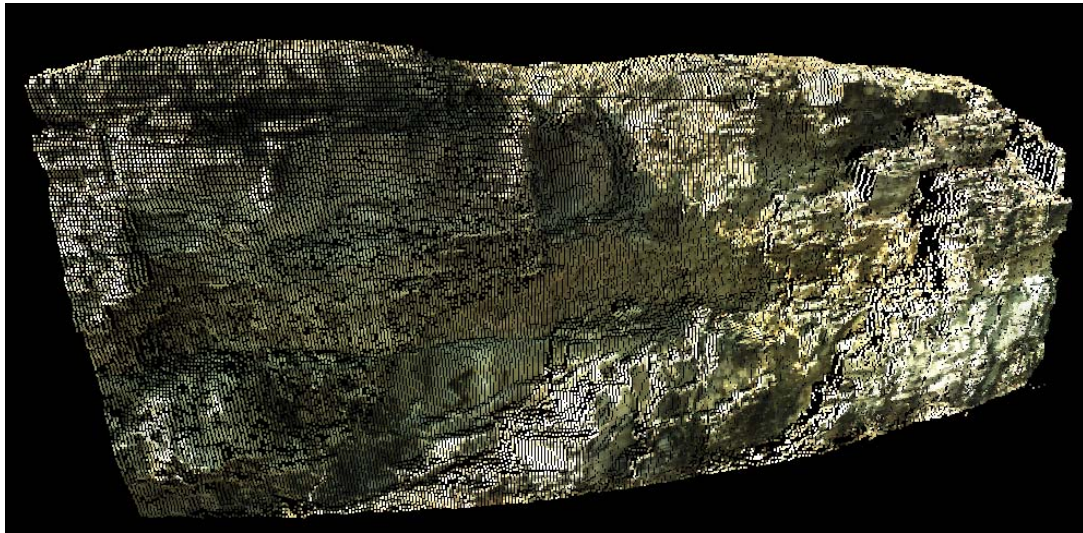


Figure 2.8. Point Cloud in XYZRGB Format (Site 1).

2.4. USING LIDAR FOR SLOPE STABILITY ANALYSIS

This section will provide a case study which used LiDAR for slope stability analysis. The research for this thesis has different applications for using LiDAR in slope stability, but the capabilities and idea of using LiDAR is the same.

At Afternoon Creek, Washington, on November 9th, 2003 a major rockslide occurred. Approximately 750,000 m³ of rock slid down the slope, some portions falling more than 600 meters in elevation onto Washington State Route 20 (SR20). The unstable slope remained a concern as it threatened SR20, but the problem was that the majority of the slope was inaccessible. A few workers were dropped by helicopter on top of the unstable slope to gather data, but this proved to be dangerous and extremely costly. It was decided to use LiDAR to gather crucial information on the slope (Strouth and Hungr, 2005).

LiDAR data was gathered using an Optech ILRIS-3D laser scanner. The data gathered was visualized and discontinuity description data extracted using Split-FXTM developed by Split Engineering LLC. Twenty one scans were taken at the landslide site, where at each site the LiDAR had to be positioned on a tripod, leveled, and aimed towards the slope of interest. Plunge and trend data of the scanners line of site was recorded, for use in calibrating the point cloud with respect to true North. From the 21 scans taken, several were unusable as the data quality was poor, due to the limitations of the scanner. Table 2.2 lists the 21 scans taken and the parameters used for each one.

The work using LiDAR for slope stability at Afternoon Creek is different than the work done for this thesis. LiDAR data was primarily used for measuring joint orientation of unreachable surfaces. This provided a much safer and accurate method for gathering critical data of the rock slope. If certain steps, which are outlined in the thesis had been taken, the data which was acquired at Afternoon Creek could have not only provided joint orientation data, but the LiDAR could have been used as a monitoring device to measure the amount of slope movement or future rockfall volumes.

Table 2.2. Afternoon Creek, Washington LiDAR Data (Strouth and Hungr, 2005).

survey station/ scan	target	spot spacing	approx. distance* (m)	approx. resolution (cm)	relative quality
1/1	failure scarp	7	600	11	okay
1/2	lower slope	20	300	16	good
2/1	failure scarp	8	500	11	good
2/2	failure scarp	15	500	20	okay
2/3	failure scarp	30	500	40	okay
3/1	scanline 1	60	60	10	poor
3/2	scanline 1	20	60	3	good
3/3	scanline 1	20	50	3	good
3/4	scanline 1	20	50	3	good
4/1	failure scarp	10	1000	27	very poor
4/2	Falls Creek runout path	10	300 - 1000	8 - 27	very poor
5/1	failure scarp	10	1000	27	very poor
5/2	lower slope	10	500	13	good
5/3	Falls Creek runout path	10	750	20	okay
5/4	range test	10	> 1200	32	very poor
5/5	range test	10	> 1500	40	no data
6/1	failure scarp - zone 3	16	250	11	good
7/1	failure scarp - zone B, zone 3	20	150	8	good
7/2	failure scarp - zone 3	20	100	5	good

3. METHODOLOGY

3.1. INTRODUCTION

The field data for this project was gathered at two sites located north of Rolla, Missouri. Figure 3.1 shows a map of the study areas in relation to Rolla.

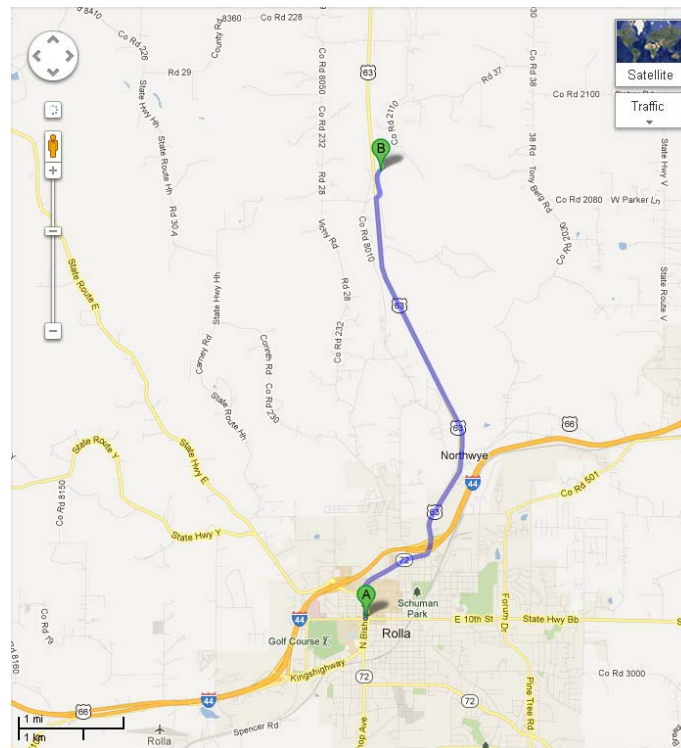


Figure 3.1. Map of Study Sites Relative to Rolla, Missouri (A is location of Rolla and B is location of the outcrops used).

The first site, which will be referred to as “Site 1” throughout this thesis, is located along Road 37 A, adjacent to Hwy 63, about three miles North of Rolla, adjacent to the Capital Quarries aggregate mine. The second site, known as “Site 2”, is located near Site 1 but inside Capital Quarries in the Northeast corner. Figure 3.2 shows the two sites relative to one another.



Figure 3.2. Map of Study Sites (Site 1 located outside the quarry and Site 2 located in the northeast corner of the quarry).

3.2. SITE SELECTION

These locations were chosen for the research study for several different reasons. The first parameter was the distance from Rolla, Missouri. The site locations had to be near Rolla since data would be collected for over a year, on a weekly basis. It was also important for the sites to be near a quarry, to investigate the affect of ground vibration (from quarry blasting) on the quantity of rockfalls throughout the year. The sites chosen are approximately 3 miles from Rolla, near Capital Quarries. Next was the safety aspect, as the user of the LiDAR unit had to be in a safe location while conducting scans. At Site 1 there is a wide ditch on each side of the small road, which has very little traffic, which provides adequate space for the user's vehicle and scanning equipment. Figure 3.3 shows Site 1 equipment setup.



Figure 3.3. Site 1 Setup (ScanStation2 placed securely on tripod, powered by EU1000i Honda generator, and operated using Cyclone software on laptop).

At this location the user would be safe from motoring traffic and possible rockfall. The Site 2 location is also quite safe, as it is in an area unused by quarry heavy equipment, and located at a safe distance from the quarry wall to protect from rockfall. At this site it is prohibited to go past the berm, to prevent possible injury from rockfall. Figure 3.4 shows Site 2 setup.

The final parameter was the evidence of current rockfall. When scoping out possible site locations, both sites had significant quantities of fallen rock accumulated piled at the toe of the outcrop. In addition to the evidence of rockfall, both of our sites are located near or within Capital Quarries, where seismic activity from blasting is recorded and can be compared to the rockfall volume amounts in Section 5.

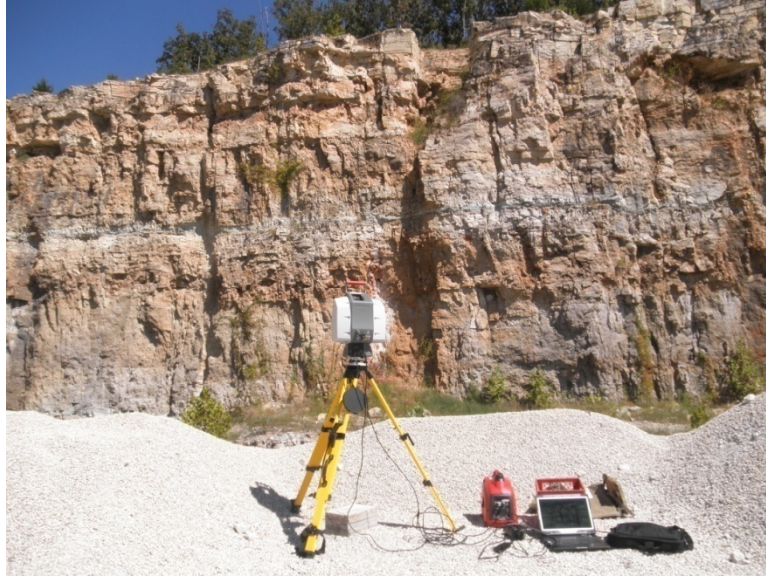


Figure 3.4. Site 2 Setup (Similar setup as Site 1, except the laptop is now operated from on the ground, and operation takes place on the berm in an unused section of the aggregate quarry).

3.3. DATA ACQUISITION

With the methods developed at Missouri S&T for collecting LiDAR data used for rockfall volume estimations, it is important that the area of interest is visible from a single location so that only one scan per site is needed. Step-by-step instructions for data collection can be found in Appendix A.

3.3.1. Equipment Needed. The equipment required for data acquisition is as follows: LiDAR scanner (ScanStation2), tripod, tribrach, generator (Honda EU1000i), laptop (with Cyclone software), LiDAR power supply, laptop power supply, and Ethernet cable. Other power sources other than a generator could be used, such as external batteries or power inverter connected directly to the motor vehicle, but the generator was the best option as it is the most reliable source and the Honda EU1000i is a very quiet generator. Additionally the generator allows the laptop to be charged simultaneously, with both easily accessible. Other LiDAR scanner models could be used for this type of data acquisition, but the ScanStation2 model provides the optical image to add the natural rock colors to the point cloud. The ScanStation2 also allows the user to input a specific sample spacing, which provides more consistent data, as well as a smaller resolution than

what the HDS6000 (the other model at Missouri S&T) could provide. The tripod and tribrach are very important for mounting the laser scanner, as the tribrach is used to secure the laser scanner to the tripod, as well as level the device. In addition to the equipment needed for acquisition, safety equipment is also needed. Hard hat, bright clothing, safety glasses, and boots are highly recommended, and required at the quarry.

3.3.2. Equipment Setup. Once at the site the first step would be to locate the position for the tripod. Registering point clouds is possible with small changes in position of the LiDAR scanner for different scans. This means that the tripod location vary up to 1 foot from the original location and the point clouds could still be correctly registered together with negligible error. To increase the accuracy of the scanner placement for consecutive scans, each site has a marker placed at the ground for centering the tripod on. At Site 1 a simple metal stake is used, which is shown in Figure 3.5.

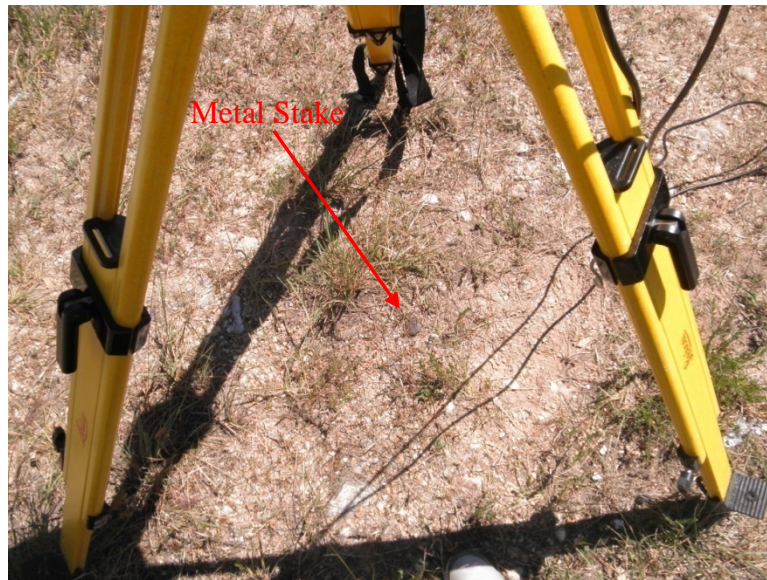


Figure 3.5. Site 1 Marker.

The tripod is positioned directly above the metal stake, with the base of the tripod at about 50 inches from the ground. The metal stake was chosen at Site 1 as the marker, because it would not cause any problem when cutting the grass and should not accidentally

be moved. All three legs of the tripod were pushed firmly into the ground to provide the best stability possible. At Site 2 a similar method is used, except instead of a metal stake, a block of wood is used as the marker for the center of the tripod. The block of wood was chosen since the area is unused by quarry operations and was easily accessible. Figure 3.6 shows the tripod placed over the block of wood at Site 2.

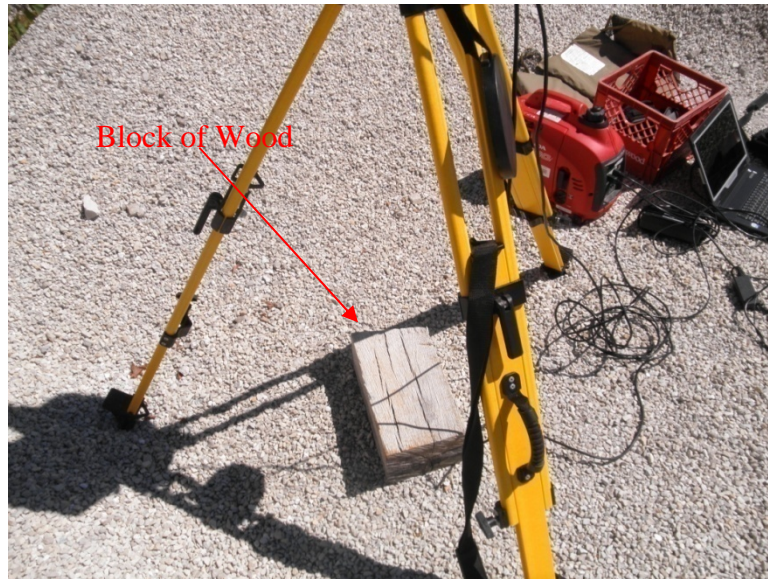


Figure 3.6. Site 2 Marker.

The same technique is used at Site 2 to estimate the height of the tripod. Using this estimation of the location and height decreases the time it takes for setting up the equipment. It is also helpful that the user acquiring the data remains constant for the life of the project, and if there are multiple users a specific measured height be used. After the tripod is set up the tribrach should be securely attached to the tripod and leveled. Figure 3.7 is an example of the tribrach used.



Figure 3.7. Tribrach.

Having the tribrach completely level is very important to ensure the datasets gathered are not tilted. It is also recommended that the optical plummet is pointed towards the rock face when attaching the tribrach, as this will allow an easier setup for the ScanStation2. Once properly attached and leveled the LiDAR scanner should be placed on the tribrach, with the power connectors and light indicators on the backside (pointed away from the rock face), and locked into place. If the setup is done like previously stated, the horizontal scan window will be at zero degrees directly in front of the LiDAR scanner. The mirror covers can then be removed and the scanner unlocked so that it can rotate freely. The generator should then be placed on the ground, with the exhaust pointed away from the work area, and started. Next, plug in the power supply into the generator and laptop so that it can start warming up, as the scanner will take about 5 minutes before it is ready to scan. While the scanner is warming up set up the laptop, and connect the Ethernet cable to the laptop and scanner.

3.3.3. Setting Parameters. Setting accurate scanning parameters will significantly save time and increase the usability of the data. The parameters should be consistent for the entire series of sequential scans, as accurate registration requires similar point clouds. The first step for setting parameters in the field would be to ensure the tripod and scanner are set in the correct location. After connected to the scanner through Cyclone an image of the area should be collected so that the Field-of-View (FOV) could be set. The FOV is very important as it constrains the area which data is gathered. Only

collecting data on the area of interest will maximize the time efficiency of the scans. At Site 1 the FOV should be set to the top and bottom of the rock outcrop for the vertical constraints, and there are two unique rock features which are used on the left and right for the horizontal constraints. The left side is a small facet rock located about 2/3 up the rock outcrop, and the left side is a small cavity located in the center of the rock outcrop, both indicated in red in the next figure. Figure 3.8 shows the extent of the FOV for Site 1.

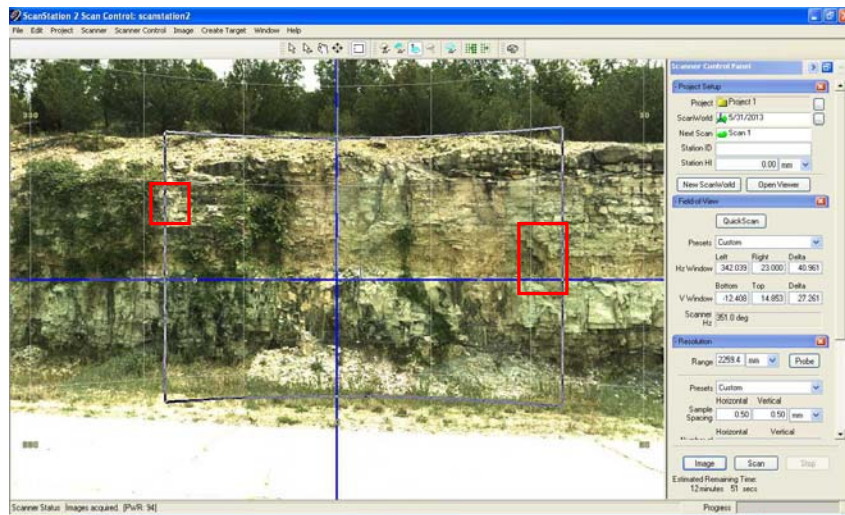


Figure 3.8. Field of View Extent of Site 1 (note the measurements on the right side are for the previously done scan and not specific to this site). The red boxes indicate the markers used for determining the horizontal extent.

The FOV at Site 2 is quite similar, where the top and bottom of the outcrop are the vertical constraints, but the horizontal constraints at Site 2 is a joint feature which runs the length of the outcrop from top to bottom on the left and a small tree on the right at the top of the outcrop, also boxed in red in the following figure. Figure 3.9 shows the extent of the FOV for Site 2.

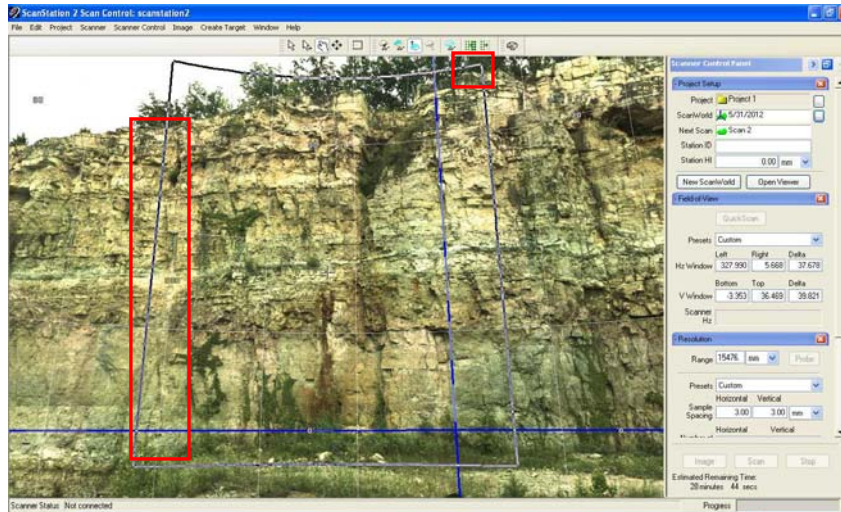


Figure 3.9. Field of View Extent of Site 2 (note the measurements on the right side are for the previously done scan and not specific to this site). The red boxes indicate the markers used for determining the horizontal extent.

Once the FOV is set for the site the center of the rock outcrop should then be probed. Probing is needed to measure the linear distance from the scanner to the center of the FOV. The distance from the scanner to the outcrop allows the LiDAR to accurately determine the spacing needed for an assigned resolution. For Site 1 the probed distance is slightly over 15 meters, and at Site 2 the probed distance is about 33 meters. After probing the resolution can be set, where Site 1 resolution is 3x3 millimeters and Site 2 is 8x8 millimeters. The difference in resolutions chosen were based on the estimated time for scanning. Site 1 is much smaller area and a 3x3 millimeter resolution takes about 12 minutes. Site 2 is larger and a 3x3 millimeter resolution would have taken over 30 minutes. Since a slightly larger resolution (8x8 millimeter) is still adequate enough to catch most differences and also reduce the time for scanning to a little less than 20 minutes, it was chosen. Once the resolution is set, Cyclone will provide an estimated time for scanning for the given site and parameters.

3.3.4. Scanning. After all the parameters are set correctly for that particular Site, scanning may commence. At Site 1 the scanning process usually takes about 12 minutes. During this time the scanner is collecting data and sending that data directly to the laptop, recording the image called a point cloud. Site 1 point cloud will usually contain approximately 9 million points, but will vary slightly depending on the extent of the

FOV. The scanning process at Site 2 takes a little longer, even though about the same number of points are collected. Scanning at Site 2 takes longer because the vertical limit of the FOV is set higher and requires the use of scanning through both the front and top window of the ScanStation2. This significantly slows down the scanning rate.

3.3.5. Exporting Data. Finally the data may be exported to a numerous number of formats for additional processing. Typically before the data is exported the digital image acquired will be applied to the point cloud, in addition to the intensity value which is set as default. At Missouri S&T the point cloud is exported into a .pts file, which is simply a common text file which lists the xyz coordinates of the point and both the intensity value of the point and the rgb data which was discussed in Section 2.3.2.

3.4. DATA PROCESSING

The LiDAR data, converted into .pts files, is processed using a series of C++ programs developed at Missouri S&T by Ken Boyko. The main objective of these programs is to clear the data of any unwanted artifacts, such as vegetation, dust particles, vehicles passing in front of the scanner, etc., and calculate the total volume difference between two subsequent scans.

3.4.1. Data Process. The entire process is broken down into 8 primary steps.

3.4.1.1 Pre-load. The Pre-Load step examines the raw pts file and determines the minimum and maximum range of the horizontal and vertical components of the point cloud. The first initial point cloud (base file) will set the boundaries for which the data is compared, which will control the subsequent loading process.

3.4.1.2 Load. This part of the process arranges the individual (x,y,z) triplets in the .pts file in order, to form a regular grid or mesh (the data in the .pts files are not ordered). The function defines bins using metadata from the Pre-Load function and loads each triplet into its proper bin. The number of points in each bin depends on the mesh resolution set by the user. If the mesh resolution is set equivalent to the scan resolution, then most bins will have a single observation. If the mesh resolution is set coarser than the scan resolution, then each bin will most likely have multiple observations. Likewise, if the mesh resolution is set finer than the scan resolution, then some bins will contain

observations while other bins may be empty. Any empty bins, or voids in the data, will later be filled in by using the Fill Gaps function discussed in the next section. Table 3.1 shows an example of the number of hits per bin, showing the number of observations (data points) per cell (set mesh resolution), and the distribution of points to bins.

Table 3.1. Distribution of Data Points

observations per cell	bins	percent of bins from total	percent of points from total
0	2937645	33.8	0.0
1	4185632	48.1	54.6
2	1303677	15.0	34.0
3	233200	2.7	9.1
4	35070	0.4	1.8
5	6104	0.1	0.4
6	1055	0.0	0.1
7	54	0.0	0.0
8	15	0.0	0.0

3.4.1.3 Fill gaps. After the initial Load function, there are often many empty bins. The Fill Gaps function identifies the empty bins and fills them using linear interpolation from the nearest surrounding edges. Only real observations can be used to calculate linear interpolated values, to prevent synthetic observations being created by other synthetic observations. Figure 3.10 is an example of the outcrop data before and after the fill gap function is completed.

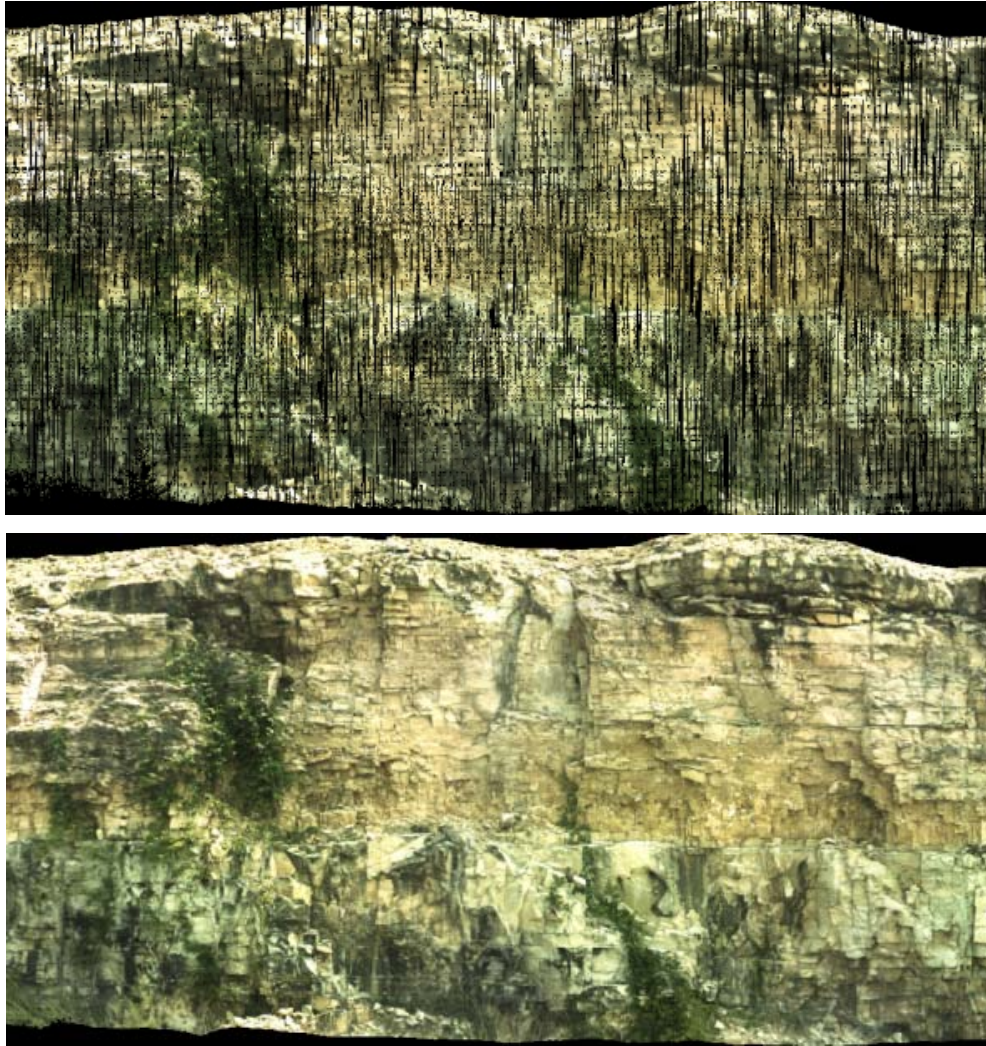


Figure 3.10. Outcrop Data Before (Top) and After (Bottom) the Fill Gap Function.

3.4.1.4 Registration. Registration orientates two point clouds to a single datum. This is required even though the reposition of the LiDAR unit is made as consistent as possible each week. The average positional recovery accuracy for weekly observations is estimated to be 200 mm horizontal, 100 mm vertical, and an angular observation within 5 degrees for all three axes. The high precision obtained from registration is required for the surface differencing process to produce reliable and accurate results. The registration process begins with a split screen where the user selects points from the baseline data and then the later corresponding data. After a conjugate control point is selected (red cross) on both the left (base date) and right (current date) windows, a correlation image is

provided to the user - illustrating the relative correlation coefficients for a small area around the current date pointing. A bright central spot indicates a unique control point - all other local areas have lower correlation coefficients. Figure 3.11 shows the split screen used for registration.

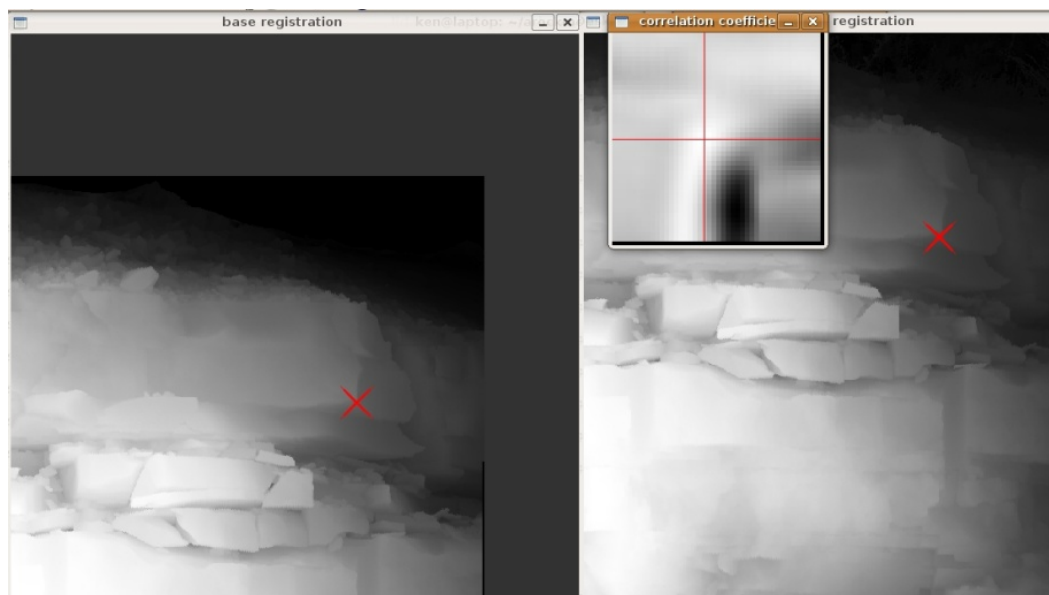


Figure 3.11. Split Screen Registration Process. The red X indicates location where the user has selected in each image, and the smaller box shows how well the two points correlated with one another.

An area-based image correlation based on surface topography is used to find the "best match". Both manual pointings and correlated pointings are retained for later use in a 7-parameter conformal 3-D transformation. This transformation allows translation in x,y, or z, rotation about the x,y,or z axis, and a universal scale factor. The transformation does not permit any differential stretching, skewing, or warping of the 3-D surface. After 4 conjugate control point pairs are selected, two transformation solutions are computed - one based purely on the manual pointings, and another based on the correlated pointings. The user is presented with the resultant root-mean-square error (RMSE) statistics for both solutions. If the best of these two solutions indicates an overall RMSE lower than the established maximum for that site (4 mm max for site 1,

and 10 mm for site 2), the user can choose to proceed with the transformation - which will use the better of the two solutions. If the overall RMSE exceeds the established maximums, the user can choose to restart the registration process for that dataset. A configuration file is written to retain the observations which were used for the final 3-D transformation.

3.4.1.5 Vegetation detection and removal. Before difference surfaces can be created, all non-rock artifacts must be removed. Artifacts could include anything from cars which pass in front of the scanner to birds or insects, or the vegetation and roots which cover the rock features. Often non-rock artifacts are represented in the data as narrow spikes. These spikes can be detected and removed by using a virtual articulating conical probe. The user defines the cone solid angle, probe length, and articulation limit which is determined as the set properties for the particular data set. The probe is dragged across the inside face of the surface, and attempts to reach every cell. Every cell that can be reached by the probe tip and doesn't intersect any other part of the surface is considered to be a real rock. If the probe cannot reach a cell it articulates in a spiral pattern in an attempt to reach the cell. The articulation allows for corners and edges of rocks to be reached and thus, be classified as “rock”. If the rock corners could not be reached, they would be classified as vegetation and deleted – resulting in rounded-off rock edges. Figure 3.12 shows the probe filter along with the parameters which have been chosen for this project, as well as the result from when probe filter is set to zero.

As can be seen in Figure 3.12, the vegetation is detected, but some of the rock edges are also detected. Using this setting would cause rounding of the rock edges and significant error in the determination of rock volumes. The parameters used are determined by trial and error to find which works best for the amount of vegetation at the sight. The probe filter is extremely time consuming, and to save CPU processing time a roof filter is used prior to the conical probe filter. The roof filter is a simple low-pass filter that operates by running a circular kernel over the surface and replacing the center cell value with the difference between that cell value and the farthest cell value within the kernel search area. This process identifies all the high frequency parts of the surface - which includes all the artifacts caused by objects passing in front of the LiDAR during the scanning process (vehicles, flying insects, and blowing leaves), all vegetation

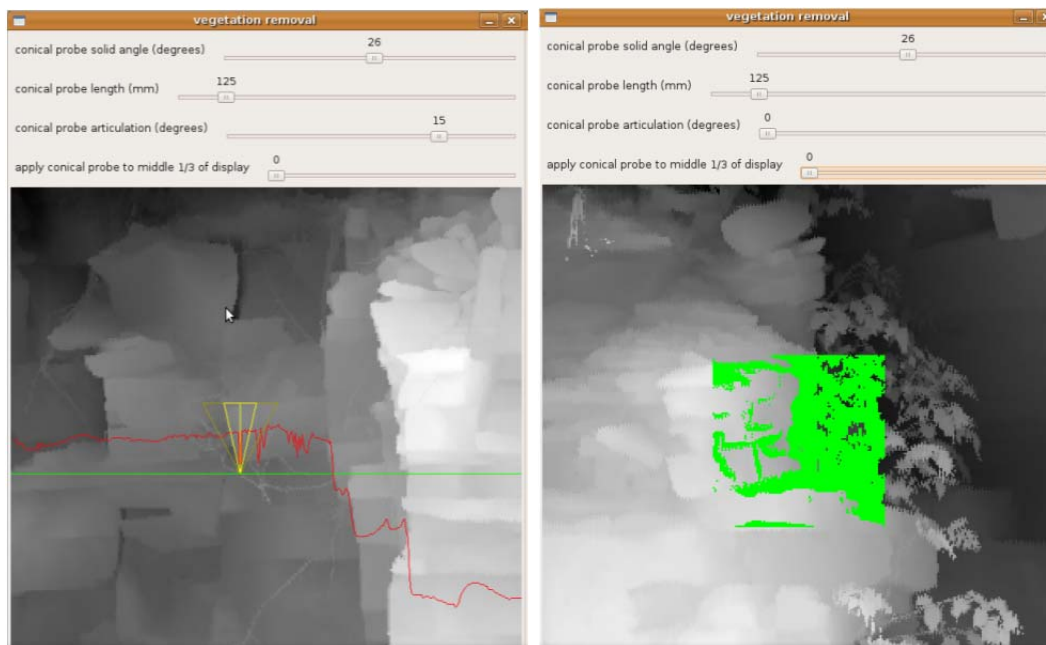


Figure 3.12. Vegetation Removal Filter. Conical probe detecting vegetation (Left) and conical probe articulation set to zero (Right).

artifacts, and (unfortunately) rock edges. Cells which are identified by the roof filter may be artifacts, but cells not picked up by the roof filter are guaranteed to be legitimate rock surfaces, so they need not be re-examined again by the more discriminating, but time-consuming articulating conical probe filter. As a result, the conical probe filter only has to process about 5% of the total data and deletes only artifacts from the rock surface. After this process, the new gaps where the vegetation was are filled using the technique described in Section 3.4.3. Figure 3.13 shows an example where vegetation has been removed.

3.4.1.6. Difference surface creation. After all artifacts have been removed and the gaps filled, difference surfaces are created by subtracting one surface from another. For this thesis the goal was to determine the volume difference caused by rockfall. To obtain this data a “difference surface” is generated by subtracting a “later” dataset from the “base date” dataset for that site. On this “difference surface”, missing rocks will be represented as areas with negative distances. Despite the tight registration and

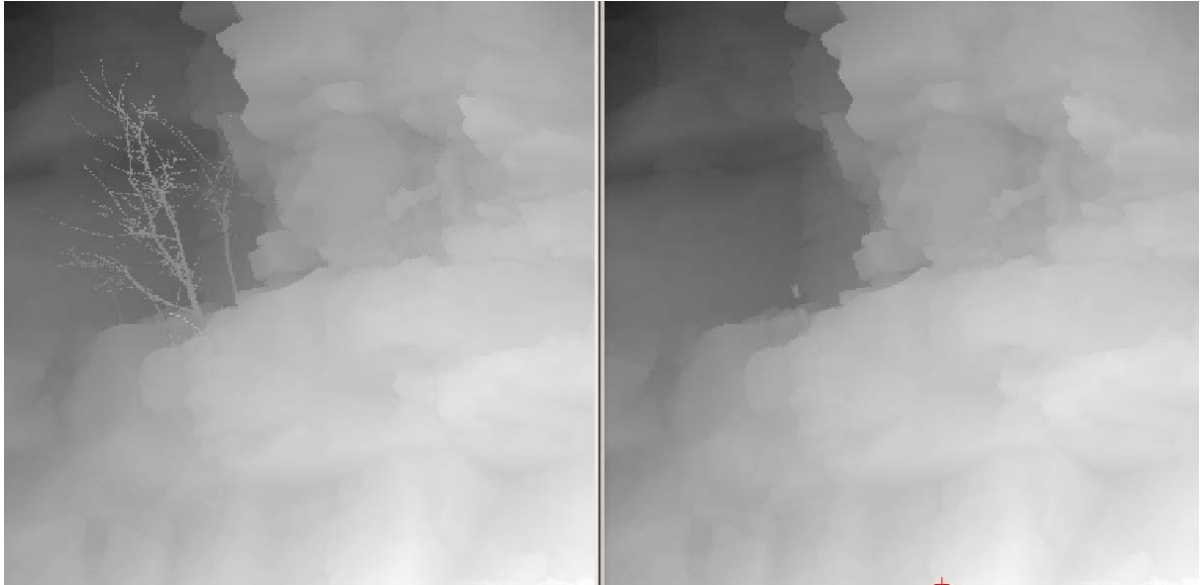


Figure 3.13. Example of Successful Vegetation Removal.

parameters set for data acquisition, the difference surfaces still contain significant artifacts, and must require additional processing.

3.4.1.7. Rock segmentation. The raw difference surfaces which still contain artifacts must be separated from the real surface differences which represent the loss of material occurring between the two dates. The artifacts are caused by several factors, such as: residual registration error, parallax errors, and shadow effects. Figure 3.14 illustrates a color-coded raw difference surface image.

Green represents areas of little change, blue indicates areas of lost volume (fallen rock locations), and red indicates areas of gained volume. Note that heavy vegetation is characterized by areas of alternating red and blue - this is caused by the movement of the vegetation between the two source LiDAR point cloud acquisitions. Thin blue or red lines are evidence of shadow and/or parallax-induced artifacts. Fuzzy repeating angled blue lines on the left side of the image are most likely small residual errors due to mechanical characteristics of the LiDAR scanning instrument. A series of processing steps are run to separate true rocks from the artifacts in the difference surface:

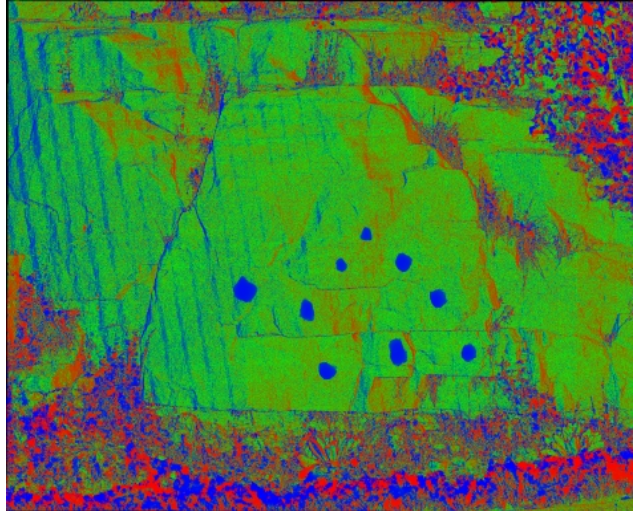


Figure 3.14. Raw Difference Surface Image.

- The area is cropped using horizontal and vertical min-max values defined in a configuration file for each site. This ensures that the areal extent of the difference surface is identical for every dataset.
- A mask, representing the fallen rocks from the next later dataset is applied. The datasets are processed in reverse time sequence, with a mask being generated for all the fallen rocks for that date. Assuming that once a rock has fallen, it should remain missing, the strategy of processing the datasets in reverse time sequence ensures that the area covered by fallen rocks accumulates positively over time.
- A thickness filter is applied to identify negative surface differences (loss of rock) greater than a threshold value - to eliminate inherent random noise in the difference surface.
- A connectivity filter is applied - enforcing the idea that a cell (representing a potential fallen rock) not only meets a size criteria, but is adjacent to at least 5 other potential fallen rock cells. This differentiates rocks versus noise based on connectivity.
- Inside rule filter: Any cell surrounded on all four sides by potential rocks is probably a rock (this eliminates single cell holes)
- A series of erodes and dilate operations are conducted to eliminate interior holes and dangling whiskers.

Finally, after all the filters have been applied, the volume is calculated, and a mask is generated representing the areas covered by fallen rocks for use in processing the next dataset.

3.4.1.8. Volume determination. After all the real rocks have been determined they are summed and this value is the volume loss over the period between the two scan dates.

3.4.2. Production and Development Environment. All software is developed in C++ , compiled using GCC© (GNU compiler collection), and runs on Ubuntu© Linux. Two open-source libraries are used for graphic output – OpenCV (Open Source Computer Vision Library) for graphic output and OpenGL™ for interactive display functions. This section describes how the processing is setup and done, including the directory structure, parameter tuning, batch scripts, batch log files, and archival back-ups.

3.4.2.1. Directory structure. For each major functional step, a directory structure captures versions of each dated data set. Log files containing run-time status information, and diagnostic graphics generated at each step are also retained to aid in analysis of errors and trends.

An identical directory structure was created for each site. Each folder in the root site directory held all the dated observations for a given stage of processing. This facilitated re-running of the whole set as improvements were made in the software. Configuration files which pertained to all dated observations were held in the root site directory.

3.4.2.2. Parameter tuning. Several functions are controlled by tuning parameters which control the behavior of that function for a particular site. To maintain consistency of the batch processing of all data sets, a single parameter file is used for all the data of a particular site. This prevents human bias from accounting for any volume differences, since the single parameter will be used throughout the research. The user determines which parameters will be used by testing the data and seeing which values work best for several different data sets. The parameters are then held constant and unique for each site.

3.4.2.3. Batch scripts. For each major function, BASH (Unix) shell scripts have been developed which run all dated datasets (dates defined in dates.config for each site) through that function. Abnormal terminations are trapped and reported by each script.

3.4.2.4. Batch log files. Run-time status information, normally sent to the console for interactive tasks, are redirected to a log file during batch runs. These log files are time-stamped, facilitating post analysis of all production runs.

3.4.2.5. Back-ups. All data is periodically back-up on two separate external terabyte drives – one stored in the office, and the other stored off-site. Archiving the data on other media is not practical due to the extremely high data volume. Each site consists of dozens of files for each of the 44 different scanning dates – resulting in over 1300 files and 105 GB for each site. It would require 45 DVDs to archive all the data for this study.

3.5. VOLUME ACCURACY

3.5.1. Water Immersion Test. A trial run using two different rocks to test the accuracy of the LiDAR volume computation was performed. For this test, an outcrop was selected, which had at least two blocks which were loose but still fit in the area which they came from without much air space between them and the outcrop. The blocks had to be in a location which was directly visible by the LiDAR scanner, so that when removed the scanner could see the entire void area. LiDAR scans were done with the blocks intact and then rescanned after the blocks were removed. Figure 3.15 shows the rock while still in place and being removed.

The data processing discussed in Section 3.4 was done to estimate the volume of the two blocks. Afterwards the two blocks were taken into the lab to run a water immersion volume test. A small container was filled with water and the blocks carefully placed into the container to determine how much water they displaced, effectively estimating the volume of each block. The two blocks were immersed separately to provide two independent test results. Figure 3.16 shows the setup of the water immersion test.



Figure 3.15. Rock Which is Used for Volume Test.



Figure 3.16. Water Immersion Volume Test.

It is very likely that the water immersion test has some error, as the surface tension of the water could potentially continue to pull some water through the tube. Also the rock itself could have adsorbed some water, reducing the total amount of volume estimated from the water immersion. The rocks in the field also could have had some error, as there was a small air gap between the rocks and the outcrop. To account for this, an estimation was made of the possible volume of the air gap. Figure 3.17 shows the measuring of the air gap in the field.

The data from each test was compared to one another. For the smaller rock the percent difference was 7.7% and for the larger rock was only 4.5%. Table 3.2 shows the results from the volume accuracy test.



Figure 3.17. Air Gap Measurement.

3.5.2. Clay Rockfall Simulation. The water immersion test was done towards the beginning of the research, before refinement of the data processing had begun. The clay rockfall simulation was done at the very end of the research, to really test the software and ensure the research was on the right track. For this test a known volume of clay is placed on the rock outcrop to imitate rocks. The volume of clay was calculated using a small box of known length, width, and height measurements, and the clay was carefully pressed inside to fill the box, yielding an estimated volume of 3706 ml. It was estimated from the few air bubbles visible an error of about ± 50 ml is present. Figure 3.18 shows the clay sample inside the small box and then the clay distributed onto the selected rock outcrop into nine separate pieces.

LiDAR scans are done from a single location before and after the clay "rocks" were placed on the rock outcrop. Since the LiDAR scanner isn't moved between the two scans, this represents perfect registration. The scanner is then relocated, in the same general location, just moved to imitate a re-setup on a different day, where a scan is done with the nine clay rocks are still intact (nothing changed besides location of LiDAR scanner). Next, a separate test was done where three of the clays pieces were removed while six remained on the outcrop. The volume of the three removed was calculated using a water immersion test of the clay. The final six clay pieces were then removed and another scan taken in order to compare manual registration of the data with all and none of the rocks present. Table 3.3 shows the results of the test.

Table 3.2. LiDAR Vs Water-Immersion Volume Comparison.

	Small Rock	Large Rock
Original LiDAR-based Volume	731.49 ml	2261.3 ml
Average Thickness of Compressible Nodes in Air-Gap	0.981 mm	1.811 mm
Projected Cross-sectional Area of Air-Gap	166.53 sq cm	284.68 sq cm
Computed Air-Gap Volume	16.33 ml	51.55 ml
Additional Observed Air-Gap (recorded before LiDAR results were known)	(None Observed)	7 ml
LiDAR Volume - Air-Gap Volume	715.16 ml	2202.75 ml
Volume Measured by Water Immersion	664 ml	2107.5 ml
Volume Difference (LiDAR - Water)	+51.16 ml	+95.25 ml
Percent Difference	+7.7%	+4.5%



Figure 3.18. Clay Rockfall Simulation Test Setup. Small Box Used for Measuring the Clay (Left) and The Rock Outcrop With Clay (Right).

LiDAR scans are done from a single location before and after the clay "rocks" were placed on the rock outcrop. Since the LiDAR scanner isn't moved between the two scans, this represents perfect registration. The scanner is then relocated, in the same general location, just moved to imitate a re-setup on a different day, where a scan is done with the nine clay rocks are still intact (nothing changed besides location of LiDAR scanner). Next, a separate test was done where three of the clays pieces were removed while six remained on the outcrop. The volume of the three removed was calculated using a water immersion test of the clay. The final six clay pieces were then removed

and another scan taken in order to compare manual registration of the data with all and none of the rocks present. Table 3.3 shows the results of the test.

Table 3.3. Clay Rock Simulation Results.

	Actual Volume Change (ml)	LiDAR Volume Change (ml)	Percent Error
Realistic Volume	3706 +/- 50		+/- 1.3%
Perfect Registration (9 rocks fallen)	3706	3737	+1%
Manual Registration (no volume change)	0	23	
Manual Registration (3 rocks fallen)	610	575	-6%
Manual Registration (9 rocks fallen)	3706	3648	-2%

From the results of the clay simulation test it appears that the calculated LiDAR volumes are very similar to that of the actual estimated volumes. The largest difference is from the separate test of three pieces of the clay where the actual volume of it was found by immersing them in a small beaker filled with water. It is likely that between the immersing the clay into the water and the imprecise measurements available on the beaker that more error is from the actual volume estimation than the LiDAR volume estimation. As can be seen from the results, all other volume tests done yielded percent errors less than 2%. This test suggests that the program developed for volume calculation using LiDAR data is fairly accurate. Figure 3.19 is an illustration of the rock outcrop along with the clay samples and their locations, where the red indicates location of volume change (rockfall).



Figure 3.19. Rock Outcrop for Clay Test. Baseline With All 6 Rocks (Top), Three Rocks Removed (Middle), All Rocks Removed (Bottom).

3.6. GEOLOGY, ROCK MASS RATING, AND Q RATING OF SITES

3.6.1. Introduction. Missouri geology can vary significantly depending on the location within the state. The type of rock, and particular climate play major roles in the stability of the rock, and the chance of rockfall. The geology found at the two study sites are very similar, and typical of central and southern Missouri. The Jefferson City Dolomite is the rock formation found at the two study sites. The Jefferson City Dolomite is part of the Ordovician System, and typically lies on top of the Roubidoux Formation. The Jefferson City Dolomite consists of light-brown to brown, medium to finely crystalline dolomite, and often has lenses of orthoquartzite, conglomerate, and shale. A section of the Jefferson City Dolomite is sometimes designated locally by aggregate producers as the "Quarry Ledge", which is the case for Site 2, and is often found 25 to 40 feet above the base of the formation. It is a popular rock, often used as a dimension

stone. The Jefferson City Dolomite ranges in thickness from 125 to 350 feet, averaging about 200 feet thick (Thompson, 1995). The following section will discuss the estimated Rock Mass Rating (RMR) and Rock Tunneling Quality Index (Q) for the two sites.

3.6.2. Rock Mass Rating. In 1976 Bieniawski published the Geomechanics Classification system, or better known as the RMR system. In 1989 Bieniawski made significant revisions to the system, to the system which is still used today. The RMR system is based on six parameters which deal with estimating the strength of rock masses (Hoek, Kaiser, and Bawden, 2000). The six parameters are:

- Uniaxial compressive strength of rock material
- Rock Quality Designation (RQD)
- Spacing of discontinuities
- Condition of discontinuities
- Groundwater conditions
- Orientation of discontinuities

Site 1 and Site 2 have very similar geology. Only Site 1 was rated, as the Site 2 rock slope was inaccessible due to quarry safety regulations. Figure 3.20 shows Site 1 and where the different ratings were acquired.



Figure 3.20. Site 1 Rock Outcrop Separated into Three Areas.

The uniaxial compressive strength of the rock is estimated using a rock hammer. Only areas 2 and 3 could be tested, as area 1 was out of reach. Since area 1 was inaccessible, the values assigned to it in the following section are based off of areas 2 and 3 and how area 1 appeared when compared to them. The first part tested was the compressive strength of the rock, which is estimated using a simple means estimate with a rock hammer (Hack and Huisman, 1971). Area 1 and 2 were estimated to be between 100-250 MPa, as rock would chip off when struck firmly with the rock hammer. Area 3 was slightly stronger and would reflect the hammer completely, yielding a greater than 250 MPa intact rock strength.

Next the RQD had to be estimated for the rock mass. Similarly to the strength estimations, area 1 and 2 were estimated to have a RQD between 50 and 75% whereas area 3 consisted of slightly larger blocks and had a RQD estimated of 75 to 90%. Spacing of the discontinuities varied throughout the area, but estimated to be between 60 and 200 mm in areas 1 and 2, and between 200 and 600 mm in area 3.

The condition of the discontinuities was consistent throughout the entire rock outcrop. Apertures averaged less than 1 mm, with slightly weathered walls. There was no groundwater present at either site, and majority of the joints had 45 to 90 degree slopes.

Calculating RMR yielded 73 for areas 1 and 2, and 82 for area 3. These RMR values are in the good rock range for 73 and very good rock range for 82. It is expected that Site 2 would have similar ratings, except for the shale area where the rock is expected to be significantly weaker near transition zones. Figure 3.21 shows Site 2 along with the area where a thin shale layer is present.

3.6.3. Rock Tunneling Quality Index. Barton of the Norwegian Geotechnical institute proposed the Q rating system for the determination of rock mass characteristics and tunnel support requirements in 1974. The value of Q ranges on a logarithmic scale between 0.001 to 1,000, and defined by the equation:

$$Q = \frac{RQD}{J_n} * \frac{J_r}{J_a} * \frac{J_w}{SRF} \quad (3)$$



Figure 3.21. Site 2 Rock Outcrop.

where RQD = Rock Quality Designation

J_n = joint set number

J_r = joint roughness number

J_a = joint alteration number

J_w = joint water reduction factor

SRF = stress reduction factor

The first quotient of the Q system is considered to estimate the block size. The second quotient estimates the inter-block shear strength, whereas the third quotient calculates the active stress (Hoek, Kaiser, and Bawden, 2000). The RQD was estimated to be 60 for areas 1 and 2 of Site 1 and 80 for area 3. The joint set number was estimated to be 4, meaning two joint sets were present in the rock outcrop, specifically two vertical joints at approximately 90 degrees to one another. The joint roughness was estimated to be 1.5, for irregular, planar joint contacts. Site 1 and 2 showed little joint alterations, and therefore yielded a 1.0 for the joint alteration number. Since the outcrop was completely dry, the joint water reduction value was 1.0. The stress reduction value was 2.5 for being a low stress contact near the surface, as the Q system is primarily for underground tunnel structures. Given all the data the Q rating was estimated to be 9 for areas 1 and 2 and 12

for area 3. A Q rating of 9 is considered to be for fair rock, whereas a Q rating of 12 is considered to be good rock.

Both the RMR and Q ratings are reasonable for the Site 1 rock outcrop. The rock itself was fairly strong, however did have many fractures which hurt the overall RQD but maintained rock strength.

4. DATA CORRELATION, RESULTS, AND CONCLUSION

4.1. INTRODUCTION

LiDAR data for this thesis was gathered for over a year, starting in January 2011 and ending in April 2012, with a total of 45 different scan dates. Scanning frequency depended upon working equipment and software, weather, and time availability, and therefore 1 scan per every week was not possible but was attempted. The rockfall volumes will be displayed in the next section, followed by other external information such as freeze and thaw cycles, precipitation levels, and seismic (blasting) data. Then Section 4.3 will discuss the final results along with recommendations.

4.2. DATA

4.2.1. Rockfall Volume. The rockfall volume was estimated using the procedure outlined in Section 3. The data is presented using graphs plotted in excel, where the x-axis represents the timeframe shown as Julian days, where 1 is January 1st, 2011. Table 4.1 shows the Julian date with the corresponding date, useful for better understanding of the seasons.

Table 4.1. Julian Dates.

Julian Date	Calendar Date	Julian Date	Calendar Date
45	2011-02-14	229	2011-08-17
76	2011-03-17	242	2011-08-30
89	2011-03-30	250	2011-09-07
103	2011-04-13	258	2011-09-15
110	2011-04-20	272	2011-09-29
126	2011-05-06	278	2011-10-05
136	2011-05-16	286	2011-10-13
158	2011-06-07	293	2011-10-20
174	2011-06-23	300	2011-10-27
181	2011-06-30	335	2011-12-01
187	2011-07-06	342	2011-12-08
196	2011-07-15	349	2011-12-15
207	2011-07-26	356	2011-12-22
214	2011-08-02	364	2011-12-30
222	2011-08-10	371	2012-01-06

Table 4.1. Julian Dates (cont.).

Julian Date	Calendar Date	Julian Date	Calendar Date
385	2012-01-20	433	2012-03-08
392	2012-01-27	440	2012-03-15
398	2012-02-02	447	2012-03-22
405	2012-02-09	453	2012-03-28
412	2012-02-16	461	2012-04-05
419	2012-02-23	468	2012-04-12
426	2012-03-01	475	2012-04-19

Figure 4.1 shows the incremental rockfall volume and the total rockfall volume of both sites 1 and 2.

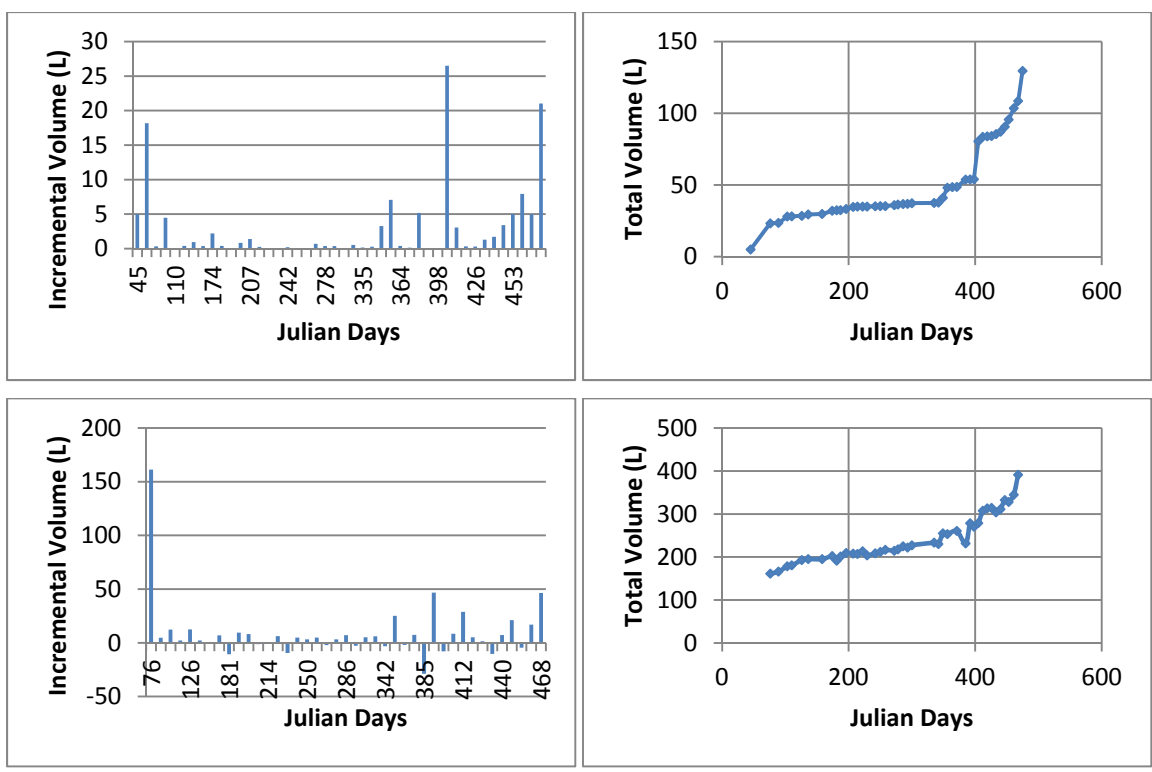


Figure 4.1. Rockfall Volume Calculated Using LiDAR. Site 1 Incremental Volume Change (Top Left), Site 1 Total Rockfall Volume (Top Right), Site 2 Incremental Volume Change (Bottom Left), Site 2 Total Rockfall Volume (Bottom Right).

The rockfall volume increments graphs above show a quantitative view of the actual amount of rockfall estimated using LiDAR. It can be seen that negative volume is recorded for Site 2 incremental volume changes, and the cause of this is still being investigated. It is possible that with Site 2 being a larger site with coarser resolution used there is just more error involved with the data. There is also possibilities that rock fell from above and landed on a shelf within the quarry where the volume of a scan is actually increased. After processing the data, Ken Boyko was easily able to create several gif images which show the actual location on the outcrop where the rock has fallen. Figure 4.2 shows three images of rockfall for both sites.

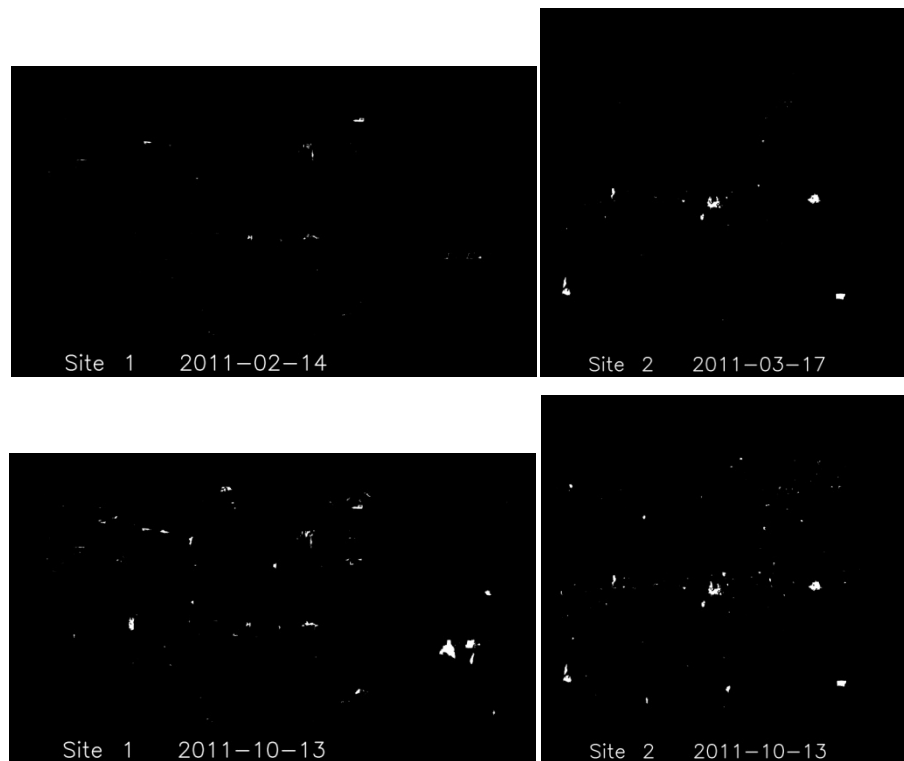


Figure 4.2. Location of Rockfall Volume. The white area represents the location of decreased volume (rockfall) between the first scan date and the date shown on the figures.

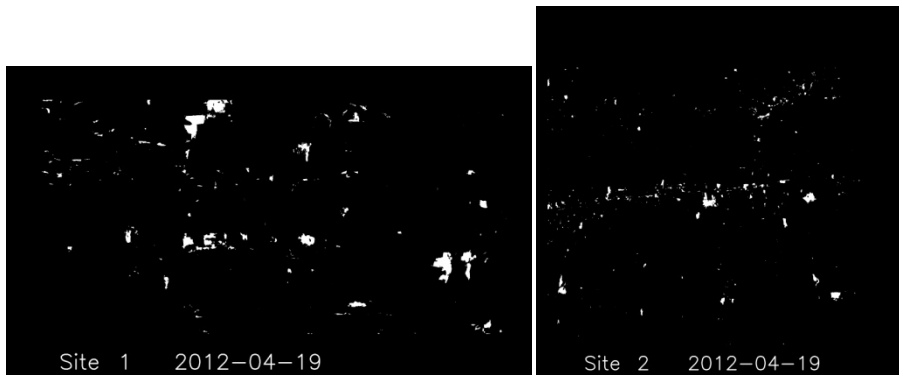


Figure 4.2. Location of Rockfall Volume (cont.).

4.2.2. Freeze and Thaw Cycles. Freeze and thaw data is very important when considering triggering of rockfall. Freezing of the water contained within cracks found in the rock will often cause expansion of those cracks, eventually causing rock fragments to ravel off the rock surface. In Missouri the freeze and thaw cycle will typically occur over several months during the winter season. For this thesis the number of times the temperature (high or low) passed the freezing point (32°F or 0°C) between the different scan dates was recorded. Figure 4.3 shows the recorded number of freeze and thaw cycles.

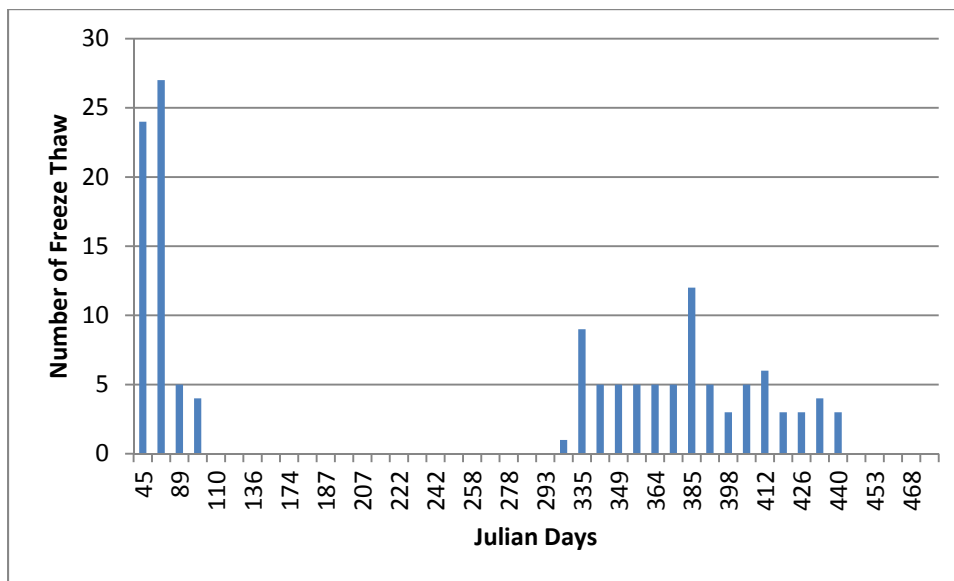


Figure 4.3. Freeze and Thaw Cycles Recorded During Each Sampling Interval.

4.2.3. Precipitation Levels. Precipitation is another major trigger of rockfall, as it slowly erodes away at material and also causes increased pore pressure. Heavy rains may cause rills to form where weaker material is located, decreasing the entire strength of that particular area. Water will also fill any cracks or small openings in the rock, removing small particles of loose rock, dirt, and organic material, increasing the size of the openings. Precipitation levels therefore play an even bigger role when combined with freeze and thaw cycles as the water found in the cracks will cause greater expansion of the openings. The other major role precipitation will cause is increased pore pressure of the rock. Water filled cavities (small openings) in rock have an overall decrease in rock strength when compared to that of similar rock without water filled cavities. While the rockfall which is being calculated is near surface, the increase pore pressure would more likely be accountable for larger scale failures, such as described in the Afternoon Creek, Washington case study in Section 2. Figure 4.4 shows the recorded amount of precipitation during each sampling interval since the beginning of data collection.

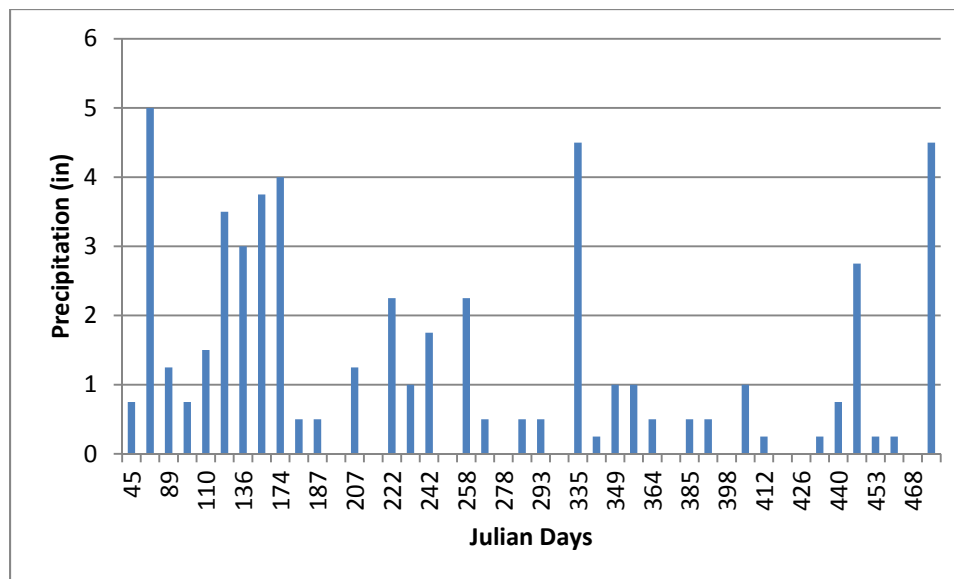


Figure 4.4. Recorded Precipitation Levels During Each Sampling Interval.

4.2.4. Seismic Data. Seismic events can often trigger rock failure. One of the primary reasons the location of Site 1 and 2 were chosen is their proximity to the local quarry. Capital Quarries records seismic data for every blast event. The seismic data recorded at the seismograph is been converted to indicate estimated strengths at the location of each of the sites using a distance relationship.

$$y_1 = y_2 * \left(\frac{x_1}{x_2}\right)^2 \quad (4)$$

Where y is the value being calculated, whether it is the peak particle velocity, peak acceleration, peak displacement, or peak vector sum, and x is the distance from the location of blast to the object (either the seismograph or site 1 and 2). Estimated values of distance were used, found by using Google Earth™. The values used are as follows: $x_1=1800\text{ft}$ (seismograph), $x_2=1750\text{ft}$ (Site 1), $x_2=1620\text{ft}$ (Site 2). Figure 4.5 shows the seismic (blasting) data acquired over the length of data collection.

4.3. FINAL RESULTS AND POSSIBLE DATA IMPROVEMENTS

4.3.1. Data Correlation. The hope for this research was to show an accurate method for calculating rockfall volumes by the use of monitoring with LiDAR. It would be expected that higher rockfall volumes would occur during or directly after large events known for causing rockfall, which have been mentioned in the previous section. Figure 4.6 and Figure 4.7 shows the graphs for Site 1 and Site 2, respectively, aligned with one another for easier comparisons.

From the volume incremental graphs, it would be expected to see some large events at the beginning of the project, and the last quarter of the project. When compared to the freeze and thaw cycle graph a small correlation can be made. This is highly expected as freeze and thaw often has one of the greatest effects on raveling rock. It was even noted when scanning during the winter months, often times rock fragments could be seen or heard falling from the outcrop. It is possible that the precipitation during these months worked in conjunction with the temperatures to cause the greater amount of

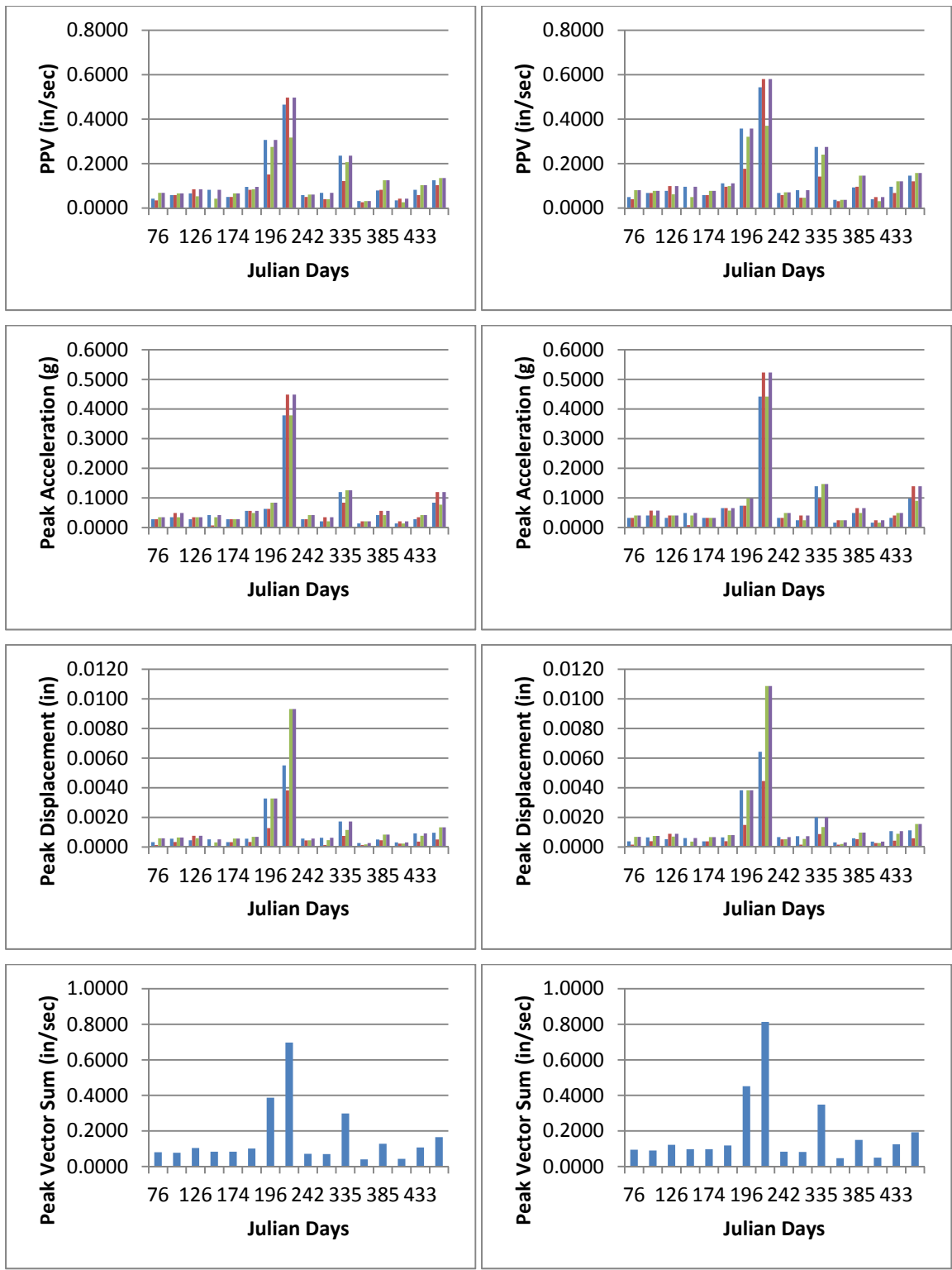


Figure 4.5. Seismic (Blasting) Data. Site 1 (Left Column) and Site 2 (Right Column). For the PPV, Peak Acceleration, and Peak Displacement: Blue=Transverse, Red=Vertical, Green=Longitudinal, Purple=Maximum. Peak Vector Sum is a Single Value and Shown in Blue for Each Recorded Blast.

rockfalls. However, several significant rainfall events during the other months had very little correlation to the rockfall volumes. On August 11th, 2011 there was a significant blast in the quarry, and large rockfall might be expected. However when comparing the rockfall volume data for that corresponding scan date, it can be seen that the smallest incremental volume was recorded. The lack of correlation suggests that the rockfall in this particular area may not be directly related to the events recorded. Some of the larger rockfall events could have been caused by the rock becoming fatigue over long periods of strain. The basic process has been demonstrated to produce accurate results under controlled conditions, as evidenced from the earlier water immersion tests and the later clay calibration tests. Further research should be done on various rock types and failure mechanisms to determine if the cause of rockfall for them correlate better with possible rockfall events.

From the volume incremental graphs, it would be expected to see some large events at the beginning of the project, and the last quarter of the project. When compared to the freeze and thaw cycle graph a small correlation can be made. This is highly expected as freeze and thaw often has one of the greatest effects on raveling rock. It was even noted when scanning during the winter months, often times rock fragments could be seen or heard falling from the outcrop. It is possible that the precipitation during these months worked in conjunction with the temperatures to cause the greater amount of rockfalls. However, several significant rainfall events during the other months had very little correlation to the rockfall volumes. On August 11th, 2011 there was a significant blast in the quarry, and large rockfall might be expected. However when comparing the rockfall volume data for that corresponding scan date, it can be seen that the smallest incremental volume was recorded. The lack of correlation suggests that the rockfall in this particular area may not be directly related to the events recorded. Some of the larger rockfall events could have been caused by the rock becoming fatigue over long periods of strain. The basic process has been demonstrated to produce accurate results under controlled conditions, as evidenced from the earlier water immersion tests and the later clay calibration tests. Further research should be done on various rock types and failure

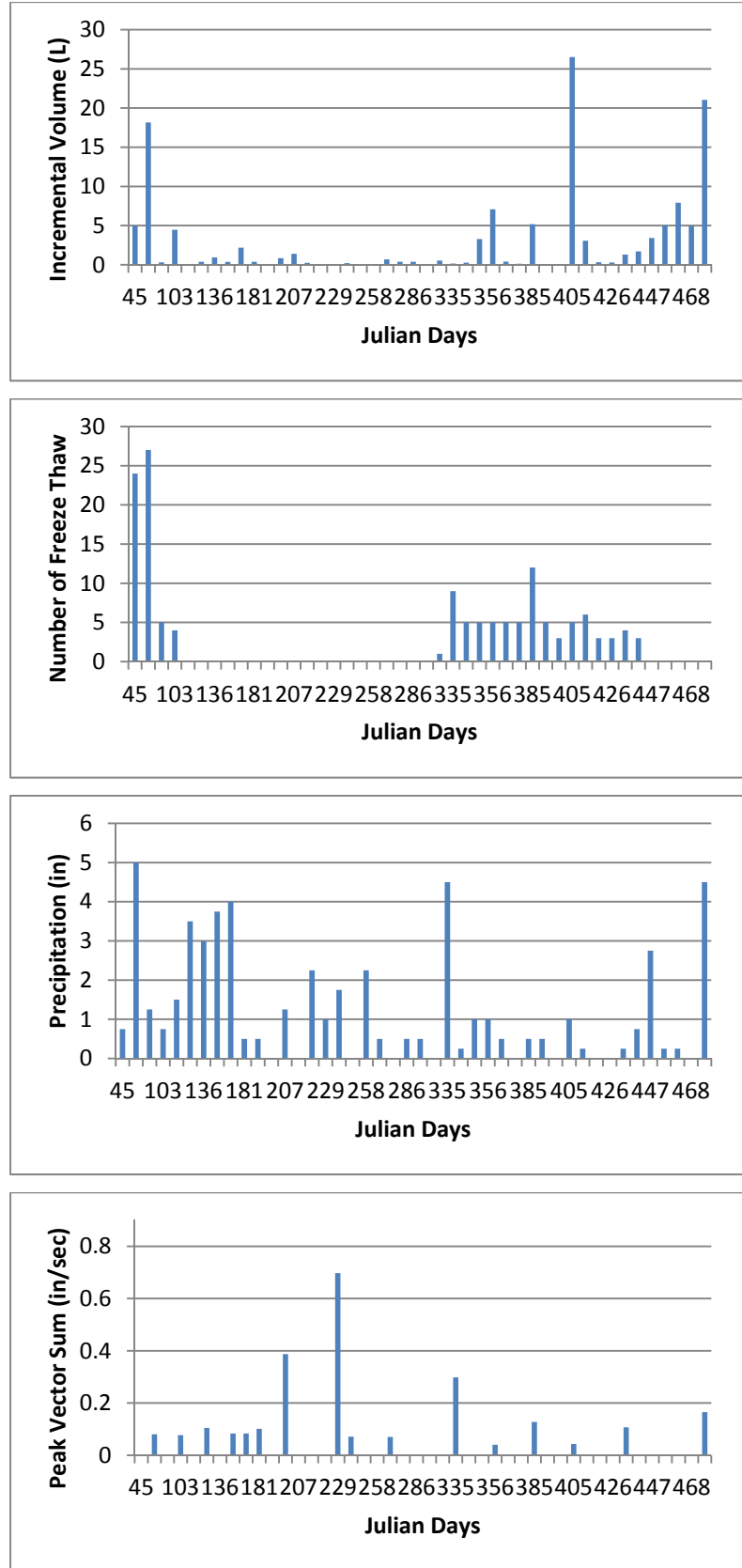


Figure 4.6. Site 1 Data Correlations.

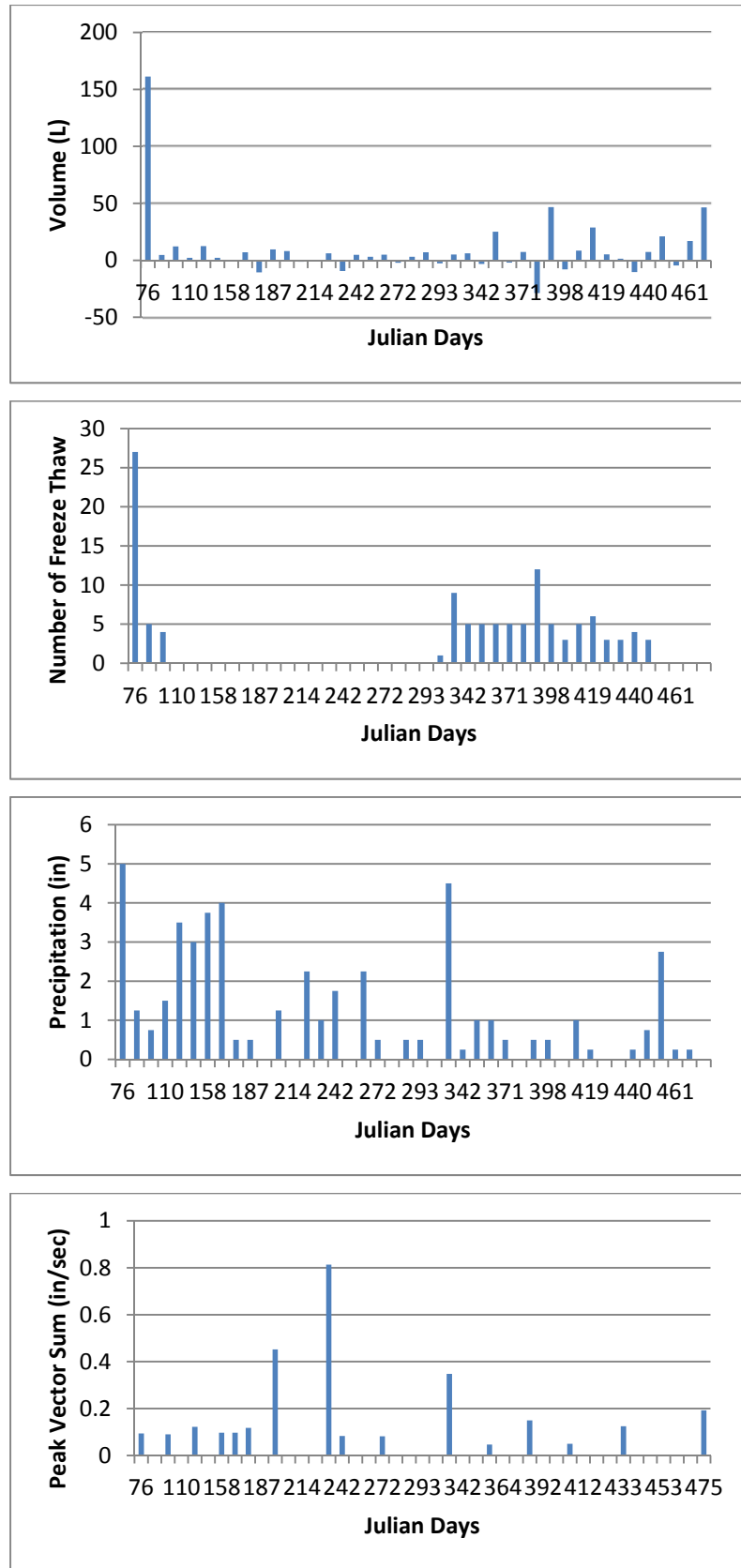


Figure 4.7. Site 2 Data Correlations.

mechanisms to determine if the cause of rockfall for them correlate better with possible rockfall events.

4.3.2. Possible Method Improvements. There are a couple suggestions for follow up research which may improve the data correlation results. Improvements could be made during scan setup, sensitivity parameter tuning, and registration. Due to time constraints these methods have not been able to be tested, but many improvements to the data processing have already been made for this thesis. Missouri S&T plans to continue data collection and working on improving the methods for better results. The following sections discuss these proposed methods in better detail.

4.3.2.1. Improved scanner setup. The data gathered for this thesis used a processing technique which would automatically align a point cloud with one another. The alignment process allowed the tripod and Lidar scanner to be setup in roughly the same location and near the same height, without the need for surveying or high precision. While the process may work fine, the setup process could be improved, being more precise on the location and height, to yield better results after realignment. Some of the error found after registration was found to be tens of millimeters off, which a better initial setup may improve. In addition, even if the registration process produced perfect 3-D residual RMSE's, even slight displacements in the setup location can produce significant "parallax" and "shadow" artifacts that can only be eliminated by tighter setup procedures.

4.3.2.2. Parameter sensitivity analysis. During the data processing parameters were chosen by the user to control the behavior of the processing filters. The parameters define various thresholds such as minimum rock thickness, minimum rock surface area, conical probe length, angle, articulation and limits, the number of erodes and dilates used to eliminate small artifacts, and other factors designed to differentiate real missing rocks from background noise and other artificial artifacts in the data. The parameters were manually tested using several different sets of data at different seasons, and were selected to be optimal for each site. Once parameters were chosen they were used for every dated point cloud, so that the data would be consistent for the project, and reduce any human error. With further research and testing it is recommended that a more in-depth sensitivity analysis and multiple parameters be done, for different seasons. The

use of multiple sets of parameters for different seasons should also be tested, as it is possible that using one set would yield less than optimal results.

4.3.2.3.Improved registration process. Several data registration techniques have been used for this thesis. The final registration process consisted of using 16 points manually selected by the user within a grid system, and then automatically correlated with other point clouds finding like points. While 16 points is significant, and leaves little room for error, further increasing this number should further increase the precision of the registration process. Improvements on the usability of the program could also be made, to make the initial selection of points more user friendly, such as the ability to deselect an accidental selection instead of having to restart the entire process. Work on completely automating the registration process should also be pursued.

4.3.2.4.Other ideas to be considered. The following ideas should be tested in an attempt to improve the quality of data and data processing:

- Generate difference surfaces between successive dates and compare the detected volume changes to those generated under the current process – which uses difference surfaces based on the difference between any given date and the base date for that site. This approach would compare incremental versus accumulated volumes.
- Acquire datasets (before and after) within hours of a significant environmental event, such as a quarry blast or large storm.
- Mask out areas of thick vegetation. The vegetation removal technique only removes thin vegetation. When vegetation becomes thick enough to entirely obscure the rock surface, it is classified as rock. This contributes to volume error due to dynamic nature of vegetation.
- Explore ways of characterizing rock versus vegetation surfaces by analyzing the fractal properties of each topographic surface. This might be used as a way of automatically generating a vegetation mask.
- Explore using color as a method for generating a vegetation mask. Although there is a slight mis-registration of the rgb color image to the topographic surface, a general mask identifying thick vegetation might be useful.

4.4.CONCLUSION

The data presented in this thesis covers the method and processing used for the research of using LiDAR for calculating rockfall volumes over time. While the entire process still needs some refinement and better understanding, the technology is definitely taking a step in the right direction. It was demonstrated with the two tests (water immersion and clay rocks) that the LiDAR process used for the research accurately estimated the volume. It would highly be recommended that research continued being done in this area, with new rock outcrops of different rock and failures types, for correlation comparison.

APPENDIX A.
STEP-BY-STEP INSTRUCTIONS FOR DATA COLLECTION

To Obtain a Scan

1. Set tripod up in desired location.
 - a. Location should be across from rock slope of interest, in a safe area from traffic and possible rockfall.
 - b. Push legs firmly into ground and bring height of the top of tripod near chest high.
2. Attach tribrach to tripod.
 - a. Face the optical plummet towards the rock slope of interest.
 - b. Level the tribrach.
3. Place ScanStation2 unit on top of tribrach
 - a. ScanStation2 power supply hookups should be faced away from the rock slope of interest, as this puts zero degrees directly center of the rock slope.
 - b. Secure ScanStation2 to the tripod.
 - c. Remove lens covers and unlatch so rotation is possible.
4. Start generator and then plug in ScanStation2 power supply.
5. Start up laptop and connect Ethernet cable from laptop to ScanStation2
6. Open Cyclone on the laptop.
7. To begin a new project a new database should be made.
 - a. On the top toolbar, go to “Configure”>”Databases...” and add a new database.
 - b. This step is only needed for the first time when starting a project, multiple scans can be done in a single database, and reused anytime.
8. Now connect to the scanner.
 - a. Go to “Scanners”>”ScanStation2” and double click.
 - b. Find the database which was made in step 7, and create a new project folder.
 - c. Highlight new project folder and select ok.
 - d. On the top toolbar, go to “Scanners”>”Connect to scanner”.
9. Once the status bar in the bottom left of the Modelspace viewer says “Connected and Ready” it is time to gather the image.
 - a. Make a rough estimate with the field of view, knowing the center of the rock outcrop of interest (the direction the optical plummet is pointing if set up correctly) is zero degrees.

- b. The field of view can be changed by either inputting numbers into the field of view window on the right hand side, or by using the fence mode located in the top toolbar (looks like a rectangle).
 - c. Once the field of view is set up, click “Image”, located at the bottom right of the modelspace viewer.
 - d. Depending on the brightness, the internal camera exposure may need more or less light. This can be adjusted by going to “Image” located on the top toolbar and selecting “Adjust Exposure...”. From here the exposure length can be increased or decreased.
10. Next the field of view can be adjusted to the image, so that only the area of interested is located within the box. This can be adjusted using the fence mode.
 11. Now probe the distance from the scanner to the center of the area of interested, by selecting “Probe” on the right side, in the “Resolution” window. Once the scanner status (located bottom left) says “Probe Completed”, change the “Sample Spacing” to the desired point distance. This measurement is the average distance between points for that probe distance. Finally hit “Scan” and wait for the scanner to finish (Scanner status at bottom left will say “Scan Completed”).
 12. If another scan is desired from the same location immediately afterwards, the user can press “New ScanWorld” located on the right hand side in the “Project Setup” window.
 13. Once scanning is completed for the day, Cyclone should be shut down, and the data can be exported back in the office.

To Export Data

1. Open Cyclone on the laptop, and find the database of interested in the SERVERS folder.
2. Open the modelspace which data is located in.
3. If rgb data is desired (image color imported onto the point cloud), go to “View”>”View Object As...” and then select “Point Cloud” in the dropdown box, then select “Color Map...”. This should open another window, where the first dropdown box (Mode) should be changed to “Colors from Scanner”. Click on “Apply” and then “Ok” and close the property window.
4. The data should be selected, go to “Selection” on the top toolbar, and “Select All”.

5. To export, go to “File”>”Export...” and select the folder the data should go to. Also change the type of file which the data will be exported to, “Text – PTS Format (*.pts)”. Then click “Save” and a new window should open. Make sure “Selected” is check marked and then click “Export”.

APPENDIX B.
DATA PROCESSING SOURCE CODE

Software Used for LiDAR Processing

Development Environment

All software was developed in-house using C++, running on Ubuntu Linux 9.4 (Jaunty Jackalope). The GCC (GNU Compiler Collection) was used for compilation. Several standard run-time libraries, such as math.h, stdio.h, and string.h, etc were also employed. Scripting was accomplished using bash (GNU Born Again Shell), copyright by the Free Software Foundation.

Two free external libraries were used for graphic display:

OpenCV – (Open Source Computer Vision Library) Originally developed by Intel, and now supported by Willow Garage. This library is free for use under the open source BSD license.

OpenGL – Registered trademark, Silicon Graphics, Inc.

Directory Structure

An identical directory structure was created for each site. Each folder in the root site directory held all the dated observations for a given stage of processing. This facilitated re-running of the whole set as improvements were made in the software. Configuration files which pertained to all dated observations were held in the root site directory.

Site-level folders:

binmasks – Binary rock masks used to facilitate the processing of data in reverse time sequence

diffSurfaces – Difference surfaces (later dated dataset minus baseline dataset)

meshed – Surface after initial load and gap filling

metadata – Min-max extent and set-up information used during initial loading

noVeg – Surfaces which have been run through the vegetation elimination program

pixColorAfterLoad – Color images of site after initial load

pixColorAfterReg – Color images of site after registration

pixColorAfterVegElim – Color images of site after vegetation removal

pixColorBeforeFill – Color images of site after load, but before gaps are filled
 pixDiff – Color coded images of raw difference surfaces
 pixIntensityAfterLoad – Intensity images of site after initial load
 pixIntensityAfterReg – Intensity images of site after registration
 pixIntensityAfterVegElim – Intensity images of site after vegetation removal
 pixMask – Binary image of rock masks used for black & white animated GIFs
 pixRocks – Fallen rocks highlighted in red on color site image – used for color animated GIFs
 pointFiles – Original point cloud data from LiDAR scanner
 registered – Surfaces after registration
 regObservations – XYZ values for the paired conjugate control points used for registration

Site-level Configuration Files:

dates.config – contains all the observation dates applicable for that site
 blobs.config – parameters defining the behavior of Rock Segmentation (sec 4.1.7)
 resolution.config – set-up information used for initial loading (mesh resolution, etc)
 vegRemoval.config – parameters defining the behavior of Vegetation Removal (sec. 4.1.5)
 volume-results.txt – summary table of volume loss for all dates in a site

File Naming Convention

Within each site sub-folder, files are named using the following convention:

yyyy-mm-dd-s.ext

yyyy: four digit year (ex. 2011)

mm: two digit month (ex. 07)

dd: two digit day (ex. 02)

s: site number (ex. 1 or 2)

ext: extension (.bin: binary surface data, .txt: text, .png: image, .pts: point cloud data, etc...)

example:

The raw point cloud data from 1-24-2011, site 1 would be named: “2011-01-24-1.pts” and would be loaded into the “site1/pointFiles” directory.

Source Code Naming Convention

xxxxMain.cpp: Main program module

xxxx.h: Class header for xxxx class

xxxx.hpp: Class Implementation for xxxx class

xx.sh: Bash script for xx function

Main Program Module Organization

Each major function defined in Section 4.1 (Data Process) was, in most cases, implemented by a single “Main” Program. In some cases, two functions were performed by a single program:

Preload – findMinMaxMain.cpp

Load and Fill Gaps– loadMain.cpp

Registration – registerMain3.cpp

Vegetation detection and removal – elimVegMain.cpp

Difference Surface creation – diffMain.cpp

Rock Segmentation and Volume Determination – volumeMain.cpp

Compilation Instructions

The GCC compilation command line is embedded in each Main Program Module. The following commands may be run in Bash to compile the Main Programs:

```
g++ -o findMinMaxMain findMinMaxMain.cpp `pkg-config opencv --cflags --libs`
```

```
g++ -o loadMain loadMain.cpp `pkg-config opencv --cflags --libs`
```

```
g++ -o registerMain3 registerMain3.cpp `pkg-config opencv --cflags --libs`
```

```
g++ -o elimVegMain elimVegMain.cpp `pkg-config opencv --cflags --libs`
```

```
g++ -o diffMain diffMain.cpp `pkg-config opencv --cflags --libs`
```

```
g++ -o volumeMain volumeMain.cpp `pkg-config opencv --cflags --libs`
```

Class Organization

The C++ language employs Classes, which are abstract structures used in object-oriented programming. Each Class is defined by a header file which describes its private data members and its private and public function prototypes. A separate file contains the implementation code for the class. Separating the definition from the implementation allows for alternative implementations without having to change the way in which the Class is used. This greatly facilitates testing and exploration in a research environment where alternative methods for the same function are being developed in parallel.

The following Classes were developed and used for this study:

dilate – dilate and erode functions used during rock segmentation

matrix – matrix operations used in transformation classes

ncc – normalized cross correlation used during registration

parm4ls – four parameter least-squares solution used during registration

probe – articulating conical probe used during vegetation detection and removal

roof – roof filter used during vegetation detection and removal

surf – general access to binary version of rock surface

transform7ls – seven parameter least squares conformal transformation used during registration

volume – rock segmentation and volume determination

Scripts

The following Bash scripts were used to process all dated datasets within each site:

load.sh – runs pre-load, load, and fill-gap functions

register.sh – re-runs registration using stored observations from interactive sessions

elimVeg.sh – runs elimVegetation using parameter file built during interactive session

diff.sh – generates all the difference Surfaces for a site

vol.sh – runs rock segmentation and volume determination functions

Source Code Listings

Source code is provided on the accompanying CD, as is organized as follows:

/main-programs/

findMinMaxMain.cpp

loadMain.cpp

registerMain3.cpp

elimVegMain.cpp

diffMain.cpp

volumeMain.cpp

/class-headers/

dilate.h

matrix.h (implementation is included)

ncc.h

parm4ls.h

probe.h

roof.h

surf.h

transform7ls.h

volume.h

/class-implementations/

dilate.hpp

ncc.hpp

parm4ls.hpp

probe.hpp

roof.hpp

surf.hpp

transform7ls.hpp

volume.hpp

/bash-scripts/

load.sh

register.sh

elimVeg.sh

diff.sh

vol.sh

BIBLIOGRAPHY

- Central Federal Lands Highway Division. "Ground-Based LiDAR Rock Slope Mapping and Assessment." Publication No. FHWA-CFL/TD-08-006. 2008.
- Duan, Y. and Li, X. "Automatic 3D Facet Orientations Estimation from LIDAR Imaging." Proceedings of 2011 NSF Engineering Research and Innovation Conference.
- Hack, R. and Huisman, M. "Estimating the intact rock strength of a rock mass by simple means." ISBN No. 0-620-28559-1. 1971.
- Hoek, Evert. "Analysis of Rockfall Hazards." *Rocscience*. N.p., 2000. Web. 12 July 2012. <http://www.rocscience.com/education/hoek_corner>.
- Hoek, E, Kaiser, P.K. and Bawden, W.F. "Support of Underground Excavations in Hard Rock." *Rock Mass Classification*. 2000.
- Hungr, O. and Evans, S.G. "Engineering aspects of rockfall hazard in Canada," Geological Survey of Canada, 1989, Open File 2061, 102 pp.
- Kersten, T.P. and Mechelke, K. "Geometric Accuracy Investigations of the Latest Terrestrial Laser Scanning Systems." Stockholm, Sweden. 2008.
- Lan, H. and Martin, C.D. "Rockfall hazard analysis using LiDAR and spatial modeling." *Geomorphology*. 2010.
- Lato, M.J. and Diederichs, M.S. "Evaluating roadside rockmasses for rockfall hazards from lidar data: optimizing data collection and processing protocols." GeoEngineering Centre: Department of Geological Sciences and Geological Engineering at Queen's University at Kingston, Ontario, Canada. 2011.
- Maerz, N.H. and Otoo, J.N. "Using LIDAR in Highway Rock Cuts." Prepared for the 63rd Highway Geology Symposium. 2012.
- Otoo, J.N. and Maerz, N.H. "3-D Discontinuity orientations using combined optical imaging and LiDAR techniques." American Rock Mechanics Association. 2011.
- Slob, S. and Hack, R. "Automated identification and characterization of discontinuity sets in outcropping rock masses using 3D terrestrial laser scan survey techniques." EUROCK 2004 & 53rd Geomechanics Colloquium. 2004.
- Strouth, A., R. L. Burk, and E. Eberhardt. "The Afternoon Creek Rockslide near Newhalem, Washington." *Landslides* 3.2 (2006): 175-79. Print

Strouth, A., Eberhardt, E. and Hungr, O. "The use of LiDAR to overcome rock slope hazard data collection challenges at Afternoon Creek, Washington." American Rock Mechanics Association. 2005.

Thompson, T. L. "The Stratigraphic Succession in Missouri." Volume 40 - Revised. Missouri Department of Natural Resources. 1995.

Wyllie, D.C. and Mah, C.W. "Rock Slope Engineering." 4th Edition. Spon Press. New York, YW. 2004.

VITA

The author, Travis James Kassebaum, was born in Creve Coeur, Missouri. He was raised west of Washington, Missouri on a small family farm. He received his Bachelor of Science in Geological Engineering from Missouri University of Science and Technology (S&T) in Rolla, Missouri in December, 2010.

Immediately after completing his bachelor's degree, the author started work on his master's degree in Geological Engineering at Missouri S&T, working under Dr. Norbert Maerz. The author worked as a Graduate Research Assistant, where he worked on using LiDAR for various projects. Some of the LiDAR projects included using the LiDAR in conjunction with a robot for military applications, funded by Fort Leonard Wood in St. Robert, Missouri. The LiDAR research even led to some valuable work experience traveling to Saudi Arabia and helping the Saudi Geological Survey (SGS) learn how to properly use a ScanStation2 for slope stability work. The author also worked as a Graduate Teaching Assistant, teaching the lab portion of Subsurface Exploration under the guidance of Dr. Maerz.

